Investigating sources of measured forest-atmosphere ammonia fluxes using two-layer bi-directional modelling

K. Hansen[1], E. Personne[2], C. A. Skjøth[3], B. Loubet[2], A. Ibrom[4], R. Jensen[5], L. L. Sørensen[6], and E. Boegh[1]

[1] {Dept. of Science and Environment, Roskilde University, Roskilde, Denmark}

[2] {AgroParisTech, UMR ECOSYS INRA-AgroParisTech, Université Paris-Saclay, 78 850 Thiverval-Grignon, France}

[3] {National Pollen and Aerobiology Research Unit, Institute of Science and the Environment, University of Worcester, UK}

[4] {Dept. of Environmental Engineering, Technical University of Denmark (DTU), Kgs. Lyngby, Denmark}

[5] {Dept. of Geography and Geology, Copenhagen University, Copenhagen, Denmark}

[6] {Dept. of Bioscience - Arctic Research Centre, Aarhus University, Aarhus, Denmark}

Corresponding author at: Dept. of Science and Environment, Roskilde University, Roskilde, Denmark. E-mail address: krihansen@gmail.com (K. Hansen), Phone: (+45) 4242 9341.

Abstract

Understanding and predicting the ammonia (NH_3) exchange between the biosphere and the atmosphere is important due to the environmental consequences of the presence of reactive nitrogen (N_r) in the environment. The dynamics of the natural sources are, however, not well understood, especially not for forest ecosystems due to the complex nature of this soil-vegetation-atmosphere system. Furthermore, the high reactivity of NH_3 makes it technically complex and expensive to measure and understand the forest-atmospheric NH_3 exchange. The aim of this study is to investigate the NH_3 flux partitioning between the ground layer, cuticle and stomata compartments for two temperate deciduous forest ecosystems located in Midwestern, USA (MMSF) and in Denmark (DK-Sor). This study is based on measurements and simulations of the surface energy balance, fluxes of CO_2 and NH_3 during two contrasted periods of the forest ecosystems, a period with full developed canopy (MMSF) and a senescent period for the DK-Sor site, with leaf fall and leaf litter build-up. Both datasets indicate emissions of NH_3 from the forest to the atmosphere. The two-layer NH_3 compensation point model SURFATM-NH_3 was used in combination with a coupled photosynthesis-stomatal conductance model to represent seasonal variation in canopy physiological activity for simulating both net ecosystem CO_2 exchange rates (R^2 = 0.77 for MMSF and R^2 = 0.84 for DK-Sor) and atmospheric NH_3 fluxes (R^2 = 0.43 for MMSF and R^2 = 0.60 for DK-Sor). A scaling of the ground layer NH_3 emission potential (Γ_g) was successfully applied using the plant area index (*PAI*) to represent the build-up of a litter layer in the leaf fall period. For a closed green forest canopy (MMSF), unaffected by agricultural NH_3 sources, NH_3 was emitted with daytime fluxes up to 50 ng NH_3-N m^{-2} s^{-1} and nighttime fluxes up to 30 ng NH_3-N m^{-2} s^{-1}. For a senescing forest (DK-Sor), located in an agricultural region, deposition rates of 250 ng NH_3-N m^{-2} s^{-1} were measured prior to leaf fall, and emission rates up to 670 ng NH_3-N m^{-2} s^{-1} were measured following leaf fall. For MMSF, simulated stomatal NH_3 emissions explain the daytime flux observations well, and it is hypothesized that cuticular desorption is responsible for the observed NH_3 emissions at night. During leaf fall in DK-Sor, ground fluxes dominate the NH_3 flux with a mean emission rate of 150 ng NH_3-N m^{-2} s^{-1}. This study shows that forests potentially comprise a natural source of NH_3 to the atmosphere, and that it is crucial to take into account the bi-directional exchange processes related to both the stomatal, cuticular and ground layer pathways in order to realistically simulate forest–atmosphere fluxes of NH_3.

Keywords: ammonia; biosphere atmosphere exchanges; compensation point; deciduous forest; measurements; modelling

1 Introduction

Predicting the surface exchange of atmospheric ammonia (NH_3) is important in order to assess the environmental consequences of the presence of reactive nitrogen (N_r) in the environment (Sutton et al. 2011). However, prediction of the NH_3 exchange between the biosphere and the atmosphere with process-based models is challenging due to the complex nature of the soil-vegetation-atmosphere system (e.g., Sutton et al. 2013). These exchange processes are controlled by a number of feedback mechanisms depending on climatic, biological, chemical and physical conditions (Flechard et al. 2013).

Atmospheric chemistry and transport models (CTMs) are recognized tools for studying the fate of nitrogen (N) in the coupled biosphere – atmosphere system (Bash et al. 2013; Pinder et al. 2008; Rao et al. 2011; Tuccella et al. 2012; Wichink Kruit et al. 2012). In the past decade, these models have been improved substantially to represent the governing processes that determine atmospheric NH_3 fluxes (e.g., Hertel et al. 2012; Hamaoui-Laguel et al. 2014; Hendriks et al. 2013). This includes the development of dynamic NH_3 emissions models (Paulot et al. 2014; Skjøth et al. 2011), detailed NH_3 emission inventories (Paulot et al. 2014; Pouliot et al. 2012; Kuenen et al. 2014; Velthof et al. 2012) and the parameterization of processes for simulating canopy NH_3 compensation points (Bash et al. 2013; Wichink Kruit et al. 2012), i.e., the atmospheric NH_3 concentrations at which the net atmospheric NH_3 flux is 0 ng m^{-2} s^{-1}.

Emissions of atmospheric NH_3 are mainly related to agriculture (Reis et al. 2009), generally as a result of volatilizations from animal husbandry, the storages and spreading of manure and mineral fertilizer (Skjøth and Geels 2013) that were found to be the dominant drivers of the spatial and temporal atmospheric NH_3 concentrations (Hertel et al. 2012; Sutton et al. 2013). However, NH_3 emissions also occur from natural sources such as from wild animals (e.g., Riddick et al. 2014; Theobald et al. 2006), forest fires (e.g., Andreae and Merlet 2001; Van Damme et al. 2014b), sea surfaces (e.g., Sørensen et al. 2003), terrestrial ecosystems (e.g., Andersen et al. 1999; Hansen et al. 2013; Sutton et al. 1997), and from the chemical partitioning of N compounds between the gas and aerosol phases (Pryor et al. 2001), but the dynamics of these natural sources are not well understood, especially not for unmanaged ecosystems (Erisman and Wyers 1993; Hansen et al. 2013; Sutton et al. 1997; Wang et al. 2011).

Atmospheric NH_3 exchange with the biosphere is bi-directional and it follows several pathways; the soil, the leaves cuticles, and the stomata (e.g., Nemitz et al. 2001). Usually, it has been assumed that NH_3 deposition occurs onto leaf surfaces and natural NH_3 emissions occurs through the stomata depending on a stomatal NH_3 compensation point (Farquhar et al. 1980a). However, the fluxes can be bi-directional for all the compartments and depend on the concentration difference between the atmosphere and the compartment. Each compartment has a varying (unitless) NH_3 emission potential (Γ) which is defined as the ratio of ammonium

(NH_4^+) to hydrogen (H^+) ions in the water (Schjoerring et al. 1998). Usually the ground is the main source of NH_3, especially in agricultural ecosystems which receive large amount of nitrogen (Nemitz et al. 2000a; Sutton et al. 2009; Personne et al. 2015; Ferrara et al. 2014). These emissions may be due to direct emissions due to agricultural operations such as application of slurry (e.g., Ferrara et al. 2016) or may also be due to the microbiological breakdown of leaf litter (Nemitz et al. 2000a; David et al. 2009). Breakdown of litter also happens in non-agricultural systems such as forests where it was found to contribute to ecosystem fluxes of biogenic volatile organic compounds (BVOCs) (Greenberg et al. 2012) contributing to feed-back mechanisms within the Earth system (e.g., Carslaw et al. 2010). Forest NH_3 emissions have been observed in late summer/autumn periods that may be related to litter decomposition and soil evaporation (Hansen et al. 2013; Hansen et al. 2015) indicating that such sources could be relevant to include in CTM models.

In bi-directional NH_3 exchange models, the unitless NH_3 emission potentials of the ground layer (Γ_g) and stomata (Γ_s) are required to simulate the NH_3 compensation points of the ground layer and the stomata, respectively (Wichink Kruit et al. 2010). Typically, these models use constant Γ-values based on measurements, however, such measurements yet only exist to a very limited extent and are demanding to conduct. Furthermore, there is a substantial need to represent dynamic growing seasons in existing CTMs (Simpson et al. 2012) in order to represent realistic seasonal vegetation and ground layer emissions of nitrogen oxide (NO), NH_3, and BVOCs. During the growing season, physiological and biogeochemical processes cause seasonal variations in photosynthesis, stomatal conductance, leaf development as well as N mobilization and translocation (Wang et al. 2013). These processes are affecting the stomatal emission potential (Wang et al. 2011) and stomatal conductance being strongly correlated with both NH_3 emission and deposition fluxes of leaves (Gessler et al. 2000). Furthermore, seasonal variation includes the dynamic development of a leaf litter layer and decomposition influencing the ground layer emission potential (Callesen et al. 2013).

The aim of this study was to investigate the contribution of the leaves and forest floor to the net NH_3 exchange at different development stages of the forest including fully developed and senescing periods. By using the two-layer bi-directional exchange model SURFATM-NH_3 (Personne et al. 2009) as a comparison and interpretation tool, the simulated fluxes are evaluated for two temperate deciduous forest reported by Hansen et al. (2013 and 2015). First, the partitioning and the temporal pattern of the net flux of NH_3 measured above the two temperate deciduous forests are presented and then, the sources of NH_3 are interpreted and discussed in relation to the phonological state of the forest canopies.

2 Methods

2.1 Experimental data and sites

The atmospheric NH_3 concentration and fluxes of NH_3, carbon dioxide (CO_2) and heat were measured at two temperate deciduous forest sites, a beech forest study site in Denmark (DK-Sor) for 25 days during late fall in 2010 (Hansen et al. 2013), and the Morgan-Monroe State Forest (MMSF) site in the central Midwestern USA for 5 days during late summer in 2013 (Hansen et al. 2015) (Table 1). The atmospheric NH_3 measurements were conducted with half-hourly temporal resolution using the Relaxed Eddy Accumulation (REA) method (Businger and Oncley 1990) in combination with Wet Effluent Diffusion Denuders (WEDD) (Sørensen et al. 1994).

2.1.1 The DK-Sor site

The DK-Sor forest is located in the central part of Zealand (55°29’N, 11°38’E). The forest consists predominantly of beech trees *(Fagus sylvatica L.)* with an average canopy height of 26 m and covers 2.5 km^2. The mean summer peak plant area index (*PAI)* in the period 2000 to 2011 was 4.6 m^2 m^{-2} with maximum *PAI* just above 5 m^2 m^{-2} (Pilegaard et al. 2011). The surrounding landscape is dominated by agricultural land use. During the 25 day measurement campaign (21 October to 15 November 2010), the measured forest canopy *PAI* (LAI-2000, Li-Cor, USA) decreased from 3.7 m^2 m^{-2} to 1.1 m^2 m^{-2} and the mean temperature was 6.7°C. Leaf fall ended on 8 November (Hansen et al. 2013) where *PAI* equalizing 1.1 m^2 m^{-2} representing trunks and branches only.

2.1.2 The MMSF site

Morgan-Monroe State Forest (MMSF) is located at 39°53’N, 86°25’W in Southern Indiana, USA. MMSF is a secondary successional broadleaf forest dominated by the deciduous tree species tulip poplar (*Liriodendron tulipifera*), white oak (*Quercus alba*), sassafras (*Sassafras albidum*), and sugar maple (*Acer saccharum*) and covers 97 km^2. The canopy height is 28-30 m and the summer peak *PAI* during 2013 was 4.6 m^2 m^{-2} (Hansen et al. 2015). Beyond the limits of the forest, the surrounding land cover is dominated by cropland. During the 5-day measurement campaign (5 September to 10 September), *PAI* was 4.5 m^2 m^{-2} and the mean temperature was 24.5°C.

2.1.3 CO_2 and energy fluxes

Carbon dioxide and energy flux observations and meteorological data used for input to the models or model validation were obtained from the European and American Fluxes Database Clusters; FluxNet (www.europe-fluxdata.eu) and AmeriFlux (http://ameriflux.ornl.gov). Eddy covariance data were gap-filled, flux-partitioned, and friction velocity (u_*) corrections were applied according to the standard procedure in FluxNet (Papale et al. 2006; Reichstein et al. 2005).

The energy flux data for the DK-Sor site needed to be filtered due to a sensitivity of the sonic anemometer that made sonic temperature fluctuation measurements at high wind speeds unreliable. Data points during periods with high wind speeds (> 5 m s^{-1}) (DOY 294–300 and 307–310) were therefore removed.

2.2 The SURFATM-NH_3 model

The SURFATM-NH_3 model (Personne et al. 2009) is a one-dimensional model that uses a two-layer bi-directional NH_3 exchange scheme including a stomatal and ground layer NH_3 compensation point. By coupling a water and energy balance model with the two-layer NH_3 resistance scheme, SURFATM-NH_3 simulates the atmospheric NH_3 flux based on measured atmospheric NH_3 concentrations, and meteorological and vegetation input (net radiation, soil and air temperature, relative air humidity, wind speed, *PAI* and rain. The model furthermore, uses predefined NH_3 emission potentials for stomata and the ground layer of the site. The scheme is based on the traditional resistance analogue describing the bi-directional transport of NH_3 governed by a set of resistances controlled by the atmosphere, r_a (s m^{-1}), the quasi-laminar boundary layer, r_b (s m^{-1}), and the canopy, r_c (s m^{-1}) respectively (e.g., Erisman and Wyers 1993). It expands the existing one-layer canopy NH_3 compensation point model (Sutton et al. 1998) with a ground layer compensation point, χ_g (mol l^{-1}), allowing emissions from the ground layer (Nemitz et al. 2001) (see Appendix A). In a similar way to the stomatal NH_3 compensation point, χ_s (mol l^{-1}), χ_g is estimated from the Henry's law and dissociation constants ($K_H = 10^{-1.76}$ (unitless) and $K_d = 10^{-9.25}$ mol L^{-1}) (Equation 1) and the dimensionless emission potential of the ground layer (Γ_g) (Equation 2).

$$\chi_g = \Gamma_g \times K_d \times K_H \times \exp\left(\frac{\Delta H_H^0 + \Delta H_d^0}{R} \times \left(\frac{1}{298.15} - \frac{1}{T_g}\right)\right) \quad (1)$$

$$\Gamma_g = [NH_4^+] / [H^+] \quad (2)$$

with ΔH_H^0 and H_d^0 being free enthalpies of acid-base dissociation NH_4^+/NH_3 (kJ mol^{-1}) and for NH_3 volatilization (kJ mol^{-1}) (Personne et al. 2009), R (0.00831 kJ K^{-1} mol^{-1}) is the perfect gas constant, and T_g (K) is the temperature of the ground layer. The model simulates the total net atmospheric NH_3 flux, F_T (µg m^{-2} s^{-1}) as a sum of each of the forest component fluxes; the stomatal, F_s (µg m^{-2} s^{-1}), cuticular, F_w (µg m^{-2} s^{-1}), and ground, F_g (µg m^{-2} s^{-1}), flux which are all related to the NH_3 canopy compensation point, χ_c (µg m^{-3}) (see Appendix A).

2.3 Model setup

The SURFATM-NH_3 model runs with a set of initialized state variables, physical parameters and constants (Table 2). As SURFATM-NH_3 was formerly applied for agricultural sites (Personne et al. 2015; Loubet et al. 2012), model parameters were adjusted to represent the two forest sites. When available, field measurements were used to set or calculate parameter values, or parameters were taken from published scientific work carried out at the sites (see references in Table 2). Otherwise, theoretical values were used (see references in Table 2), or parameters were estimated by trial-error method within a range of realistic values found in the scientific literature (see Table 2).

2.3.1 Modelling the stomatal resistance

A physiologically based leaf photosynthesis-stomatal conductance model approach proposed by Collatz et al. (1991) was used to simulate stomatal resistance (r_s). Based on dynamic coupling between a stomatal conductance, g_s (m s^{-1}) model formulated by Ball et al. (1987) (Equation 4) and mechanistic simulations of photosynthesis (Equation 5), the stomatal resistance ($r_s = 1/g_s$) was simulated and included in SURFTAM-NH_3

$$g_s = m \frac{A_n h_s}{C_s} + b \quad (4)$$

$$A_n = \min\{J_E, J_C, J_S\} - R_D \quad (5)$$

The relative humidity at leaf surface, h_s (unitless), and the CO_2 partial pressure at leaf surface, C_s (Pa), determines g_s along with leaf scale net carbon assimilation, A_n (mol m^{-2} s^{-1}), and two fixed constants (m = 7 and b = 0.01 mol m^{-2} s^{-1}) representing the slope and intercept. A_n is determined by the minimum of three potential capacities and the leaf dark respiration, R_D (mol m^{-2} s^{-1}) following Equation 5 (Collatz et al. 1991; Farquhar et al. 1980b). J_E (mol m^{-2} s^{-1}) is the light-limited assimilation rate, J_C (mol m^{-2} s^{-1}) is the rubisco-limited assimilation rate, and J_S (mol m^{-2} s^{-1}) is the assimilation rate due to the limitation of the export of assimilates inside the leaf. Measured *PAI* is used as model input to upscale leaf simulations to canopy scale (Sellers et al. 1992). Details of the coupled photosynthesis-stomatal conductance model and the soil/ecosystem respiration parameterization are described in Appendix B. The results from using the g_s model were evaluated using measured eddy covariance CO_2 fluxes (Pilegaard et al. 2011; Schmid et al. 2000) to verify *NEE* simulations. The simulated r_s estimates were then utilized for modelling the atmospheric NH_3 exchange rate using SURFATM-NH_3. The simulations were performed for the full years 2010 (DK-Sor) and 2013 (MMSF) to examine the seasonal performance of the model.

2.3.2 Emission potential of the ground layer (Γ_g) and the stomata (Γ_s)

The NH_3 emission potentials of the ground layer and stomata, Γ_g and Γ_s, were not measured at the two sites during the measurement campaigns. Therefore, measurements of Γ_s from late fall period in 2008 and 2009 from the DK-Sor site, reported by Wang et al. (2011 and 2013), were used to set Γ_s = 200 for DK-Sor representative of senescing leaves, and a constant value for MMSF of 400 was used to represent Γ_s of a green forest canopy with *PAI* close to its maximum value. In this paper, we suggest a scaling of Γ_g in the leaf fall period using *PAI* to represent N enrichment of the ground layer (soil + litter) due to litter fall:

$$\Gamma_g = \Gamma_{g,min} + \left[\left(\Gamma_{g,max} - \Gamma_{g,min}\right) \times \Delta LPAI\right] \quad (6)$$

where $\Delta LPAI = 1 - \left(\frac{PAI - PAI_{min}}{PAI_{max} - PAI_{min}}\right)$ represents the change in the litter layer derived from the measured *PAI* using the LAI-2000 sensor (Figure 1). Considering the lag time from the beginning of leaf fall until decomposition is efficient, the scaling is applied for the period with *PAI* decreasing from 3.5 (hence PAI_{max} = 3.5 m^2 m^{-2}) until it reaches its minimum value (PAI_{min} = 1.1 m^2 m^{-2}). Predefined minimum and maximum values of Γ_g are used. We set $\Gamma_{g,min}$ = 300 based on litter measurements from Wang et al. (2011 and 2013), and $\Gamma_{g,max}$ = 18000 is estimated by trial and error method to represent the higher ground layer N emission potential following the leaf fall period (Figure 1).

3 Results

3.1 Model testing for energy and CO_2 fluxes

Before SURFATM-NH_3 was applied to simulate the atmospheric NH_3 fluxes above the two forests, the model's physical representation of the ecosystem dynamics was evaluated by 1) verifying the physiological representation of the canopy by comparing measured and modelled *NEE*, and 2) comparing simulated and measured energy fluxes.

SURFATM-NH_3 was run for all days with available NH_3 flux data for this study, i.e., 5 days in the late summer 2013 (DOY 248–253) for the MMSF forest site, and 25 days during the leaf fall period 2010 (DOY 294–319) for the DK-Sor site (Figure 2).

3.1.1 Net ecosystem exchange (*NEE*)

Model simulations of *NEE* are strongly correlated with measured CO_2 flux data (Figure 3) for both MMSF (R^2 = 0.77) and DK-Sor (R^2 = 0.84), and high concordance correlation coefficients (*CCC*) further signify good agreement between data and simulations of the two sites (*CCC* = 0.72 for MMSF and *CCC* = 0.83 for DK-Sor). For DK-Sor, the stomatal activity was less towards the end of the observation period due to leaf senescence and leaf fall. Hence the modelled atmospheric fluxes were less sensitive to leaf-scale r_s variability in that period. The close agreement of the simulated CO_2 fluxes to the measured CO_2 fluxes ensures the consistent integration of the stomatal resistance r_s in SURFTAM-NH_3 model.

3.1.2 Energy fluxes

During the measurement period of MMSF, the forest *PAI* was 4.5 m^2 m^{-2}, the mean temperature was 24.3 ºC, and it rained 12.8 mm (Table 1). The rain fell within a 3-4 hour period during the night on DOY 251 (Figure 2). Over the five days, the energy fluxes showed a typical pattern for vegetated ecosystems of peak fluxes during daytime with sensible heat fluxes (*H*) of up to 200 W m^{-2} and latent heat fluxes (*LE*) of up to 400 W m^{-2}. Ignoring in-canopy heat storage and metabolic terms, the average instantaneous energy balance closure fraction $(H+LE)/(R_n-G)$ was 0.50 (Figure 4a), however accounting for the storage terms is important for the energy balance closure (Stoy et al. 2013). The model simulates the diel patterns and ranges of the energy fluxes in strong agreement with observations, i.e., R^2 = 0.78 and *CCC* = 0.69 for *H*, and R^2 = 0.87 and *CCC* = 0.78 for *LE* (Table 3).

The measurement period of DK-Sor was characterized by decreasing temperatures, leaf senescence and leaf fall. The canopy *PAI* decreased from 3.7 m^2 m^{-2} to 1.1 m^2 m^{-2} between DOY 294 and 312, and the mean temperature throughout the period was 6.7 ± 2.6°C (Table 1). *LE* was continuously lower than 200 W m^{-2}, and *H* reached a daytime maximum of 100 W m^{-2} only twice for the 25 days of observed period. The simulated reference evaporation (Allen et al. 1998) confirmed low atmospheric evaporative demand (between -50 and 100 W m^{-2}) during the rainy and overcast measurement period (Figure 2). Even though the energy balance closure (Figure 4b) and the statistical synthesis for the comparison between simulations and measurements for the DK-Sor site (Table 3) are very weak during this overcast and rainy period (i.e., R^2 = 0.17 and R^2 = 0.07 for *H* and *LE*, respectively), the typical diel pattern of the fluxes (*H* and *LE*) is clearly recognized (Figure 2).

3.2 Ammonia fluxes

At MMSF, the fluxes were positive during both day and night, indicating a release of NH_3 from the forest ecosystem to the atmosphere. The measured NH_3 fluxes showed a clear day-time pattern with maximum emissions during midday of up to 51.6 ng NH_3-N m^{-2} s^{-1} (Figure 5a), and the model represented the same day-time pattern with peak emissions during midday. The simulated range of daytime NH_3 emissions is also in good agreement with measurements during most of the period (between 36 and 46 ng NH_3 m^{-2} s^{-1}), however, the NH_3 fluxes are overestimated during midday on the last two days. During nighttime, the model simulated zero or negative net NH_3 exchange, while emissions of up to 30 ± 70 ng NH_3-N m^{-2} s^{-1} were measured.

The measured NH_3 fluxes for DK-Sor show deposition fluxes of −250 ± 300 ng NH_3-N m^{-2} s^{-1} in the beginning of the period that gradually change to emission fluxes of up to 670 ± 280 ng NH_3-N m^{-2} s^{-1} towards the end of the measurement period (Figure 5b). This change occurred due to leaf senescence and leaf fall causing a smaller canopy surface area for NH_3 depositions and possibly NH_3 emissions related to N translocation and soil emissions (Hansen et al. 2013). Contrary to NH_3 flux measurements at MMSF, no clear diurnal variation was observed in NH_3 fluxes during the leaf-fall period in DK-Sor. Fluxes turned from negative (deposition) to positive (emission) on DOY 303 at which time *PAI* had decreased from 4 m^2 m^{-2} to less than 3 m^2 m^{-2}. The mean emission rate was 150 ± 138 ng NH^3-N m^{-2} s^{-1} during the rest of the measurement period (until DOY 319). The model simulated well the measured NH_3 emissions following leaf fall, however, during DOY 314–316, a NH_3 emission event with fluxes up to 500 ± 131 ng NH_3-N m^{-2} s^{-1} was measured which was not captured by the model.

3.3 Ammonia flux contributions

The SURFATM-NH_3 model was used to analyze the contribution of the individual sources to the total flux. It was found that for MMSF (Figure 6a), the stomatal exchange was the main contributor (up to 50 ng NH_3-N m^{-2} s^{-1}) to the simulated forest NH_3 emissions during daytime. The strong stomatal control of NH_3 emissions is in turn controlled by environmental factors with a strong diel signal (radiation, temperature, humidity, CO_2). The modelled deposition to the leaf cuticles was small (up to 4.5 ng NH_3-N m^{-2} s^{-1}) and predominant during the night when the other components were less active, and relative air humidity was high. The modelled ground layer only contributed with small emissions during day time (up to 1.5 ng NH_3-N m^{-2} s^{-1}). The observed nighttime emissions were not simulated by the model.

For DK-Sor, during leaf fall (Figure 6b), the diurnal pattern differed substantially from that of the green canopy of MMSF. Here, the ground layer, or more specifically the fresh decomposing litter layer, was by far the largest contributor (up to 150 ng NH_3-N m^{-2} s^{-1}) to the total simulated NH_3 emissions from the forest to the atmosphere. Depositions (up to 30 ng NH_3-N m^{-2} s^{-1}) to the cuticular surfaces were simulated for DK-Sor whereas stomata were inactive during most of the measurement period due to advanced leaf senescence, and hence did not contribute significantly to the regulation of the NH_3 flux. The NH_3 fluxes thus showed a less pronounced diel pattern (Figure 6b) with slightly higher emissions during daytime (average of 91 ng NH_3-N m^{-2} s^{-1}) as compared to nighttime (average of 70 ng NH_3-N m^{-2} s^{-1}).

3.4 Model sensitivity to the emission potentials

The sensitivity of the simulated mean diel NH_3 flux to the emission potentials for leaves (Γ_s) and the ground layer (Γ_g), respectively, was examined for the different phenological stages represented by the two studied forests. For this purpose, a range of 0-1000 was chosen for Γ_s

and 0-30000 for Γ_g as inputs for SURFATM-NH_3 modelling. The modelled NH_3 fluxes of the green forest canopy were sensitive to Γ_s (Figure 7a), but this was not the case for the senescing forest canopy (Figure 7b) with *PAI* decreasing from 3.7 m^2 m^{-2} to 1 m^2 m^{-2} (Figure 1). During and after leaf fall, the modelled NH_3 fluxes of DK-Sor were very sensitive to Γ_g, while the sensitivity of NH_3 fluxes to the large range of Γ_g input values is less for MMSF (Figure 7c and 7d). Due to the use of *PAI* for scaling Γ_g in this study (Equation 6), Γ_g will however remain low (close to $\Gamma_{g,min}$) for a green closed canopy such as MMSF, and this causes also the simulated soil NH_3 fluxes to remain low (Figure 6a) irrespective of the parameter value set for $\Gamma_{g,max}$. In contrast, the simulated NH_3 fluxes of senescent forests (e.g., DK-Sor) will remain very sensitive to the chosen parameter value for $\Gamma_{g,max}$, and the soil NH_3 emission contributes significantly to the canopy NH_3 fluxes in this case (Figure 6b).

4 Discussion

This study aimed to analyze contributions of measured NH_3 fluxes from individual forest compartments (ground layer, cuticle and stomata) and to quantify these individual contributions to the net forest - atmosphere NH_3 flux for two deciduous forests showing distinct diurnal (MMSF) and non-diurnal (DK-Sor) NH_3 flux patterns indicative of forest NH_3 emissions. The distinct diurnal and non-diurnal flux patterns may be related to dominant processes influencing forest NH_3 emissions in different phenological phases and in different landscape settings. In particular, MMSF is located in a remote region while DK-Sor is located in an agricultural region characterized by large atmospheric NH_3 depositions in the growing season (Hansen et al. 2013). Thus, only MMSF (not DK-Sor) show NH_3 emissions in the green (mid-season) period, and only DK-Sor (not MMSF) show NH_3 emissions in the leaf-fall period (see Hansen et al. 2013; 2015). In order to analyze the sources of the observed NH_3 flux emissions of the two different (remote and anthropogenic) deciduous forests, we used the biophysical bi-directional surface model SURFATM-NH_3 in combination with a physiologically based leaf photosynthesis-stomatal conductance model (Collatz et al. 1991) for simulating the NH_3 and CO_2 fluxes in different phenological stages. The good agreement for the energy and *NEE* fluxes between measurements and simulations gives confidence in the model representation of the physical and physiological processes that are important for simulating and analyzing the observed forest - atmosphere NH_3 exchange.

4.1 Forest – atmosphere NH_3 fluxes

4.1.1 MMSF – a natural green forest canopy

Overall, the daytime magnitude of the NH_3 fluxes from the green canopy at MMSF (up to 50 ng NH_3-N m^{-2} s^{-1}) and the diurnal pattern of the NH_3 fluxes from the forest were simulated moderately well with SURFATM-NH_3 (R^2 = 0.45). In particular, daytime stomatal NH_3 emissions are well simulated (in the range 36 and 46 ng NH_3 m^{-2} s^{-1}), however slightly overestimated during midday, whereas measured nighttime NH_3 emissions (up to 30 ng NH_3-N m^{-2} s^{-1}) were not represented by the model (Figure 5a). Nighttime emissions of NH_3 are rarely reported in the scientific literature because deposition fluxes exceed emission rates in most studies. Exceptions are crop fields and managed grasslands where fertilization causes NH_3 volatilization from soil and fertilizers during both day and night (e.g., David et al. 2009; Sutton et al. 2009). In contrast, the MMSF station represents a remote natural site with very low atmospheric NH_3 concentrations (≈ 0.5 µg NH_3-N m^{-3}) and inferior NH_3 deposition (Figure 6a). If the atmospheric NH_3 concentration is lower than the NH_3 compensation point, natural ecosystems may act as a source of NH_3 (Langford and Fehsenfeld 1992). Sites with low N supply are generally expected to have low NH_3 compensation points (e.g., Massad et al. 2010a; Zhang et al. 2010). The sources of NH_3 emissions are further discussed on the basis of observed and modelled NH_3 emissions in section 4.2.

4.1.2 DK-Sor - a senescent forest influenced by anthropogenic NH_3 depositions

For DK-Sor, NH_3 depositions up to 250 ng NH_3-N m^{-2} s^{-1} were measured during the first five days when *PAI* was ~ 3 m^2 m^{-2} (Figure 5b). The model was not able to represent these deposition rates. Indeed, the measurements exceed the maximum possible flux permitted by turbulent transfer (F_{max} = $-c_{NH3}/r_a$) in this period, as discussed in Hansen et al. (2013), however this simple analysis assumes horizontal and vertical homogeneity and no chemical reactions within the gradient. Following these days, emissions of up to 670 ng NH_3-N m^{-3} were observed during the leaf fall period. The emission events during DOY 306–308 and 316–318 are well simulated by SURFATM-NH_3 using *PAI* to scale the influence of litter on the ground layer emission potential. Modelled emissions were strongly controlled by turbulence assessed by the friction velocity. However, the emission fluxes measured during DOY 314–316 are not captured by the model. During these days, the air temperature decreased to below 5°C, and on DOY 316 it increased to above 5°C. The low temperatures are limiting the modelled emissions from the ground layer, as the compensation point depends strictly and exponentially on temperatures (Husted and Schjoerring 1996; Mattsson et al. 1997).

4.2 Sources of forest - atmosphere NH_3 fluxes

Simulated forest component NH_3 fluxes (Figure 6a) show that, for MMSF, NH_3 emissions up to 50 ng NH_3-N m^{-2} s^{-1} dominate the daytime net flux due to stomatal release of NH_3 from the leaves, whereas the contribution of simulated soil emissions is insignificant. SURFATM-NH_3 simulates very little cuticular absorption during night and morning, but relatively high observed NH_3 emissions at night suggest that cuticular desorption is more important (section 4.1) and responsible for nighttime emissions up to 30 ng NH_3-N m^{-2} s^{-1} for this dense natural forest ecosystem.

For DK-Sor, being a small forest surrounded by intensively cultivated crop fields, emissions up to 150 ng NH_3-N m^{-2} s^{-1} were observed in the leaf fall period corresponding to approximately 130 % of the net flux at midday. During/after leaf fall, the ground layer contributes almost solely to the modelled NH_3 emissions (Figure 6b). Stomatal NH_3 fluxes are insignificant in the leaf fall period but the average cuticular absorption amount to 30 ng NH_3-N m^{-2} s^{-1}. Due to the cold and humid weather (Table 1), modelled cuticular deposition is nearly constant with no diel variation.

Less knowledge exists about soil and litter emissions of NH_3 in (semi-)natural ecosystems. Both emission pathways depend strongly on the seasonal variation in canopy physiological functioning and the building of a leaf litter layer on the forest floor that potentially contributes as a source for NH_3 emissions.

4.2.1 Ground layer NH_3 emissions

Walker et al. (2008) measured the soil NH_3 emission potential of a forest exposed to large NH_3 deposition and found it to be 20 (n = 34) at a depth of 5 cm, however other studies indicate much higher emission potential of decomposing litter layers (e.g., Zhang et al. 2010). For instance, Wang et al. (2011) observed higher emission potential of (newly) fallen leaves (Γ_g = 300) compared to senescing leaves (Γ_s = 200) at the DK-Sor site. Since it may take 1.3-2 years before forest leaf litter is totally decomposed (Muller 2003), the seasonal development of forest floor Γ_g is however not known. Any ground layer NH_3 emissions may be absorbed by the overlying leaf layers of closed canopies (Nemitz et al. 2001; Personne et al. 2009). In case of much higher estimates for Γ_g (6000-30000) than measured for the DK-Sor forest (Γ_g = 300) by Wang et al. (2011), the modelled nighttime forest NH_3 emissions of MMSF would be sensitive to the emission potential of the ground layer (Figure 7c). Using such high estimates for Γ_g, the simulated NH_3 emissions of MMSF (Figure 7c) would however exceed the daytime NH_3 flux observations considerably (Figure 5a). Thus, the observed nighttime NH_3 fluxes of the green forest canopy at MMSF are rather caused by foliar emissions or related to transitions in the gaseous-aerosol phases of atmospheric NH_3 not included in the model.

4.2.2 Foliar NH_3 emissions

Foliar emissions during daytime are very sensitive to stomatal emission potential and stomatal conductance (Figure 7a). In this study, Γ_s was set to 400 to represent a mid-season green forest canopy, following leaf measurements at DK-Sor (Wang et al. 2011). The use of similar parameter value for Γ_s at MMSF and DK-Sor is supported by nearly similar leaf nitrogen concentration of the two sites (Table 1). During nights, this emission source diminishes due to stomatal closure, however a number of recent gas exchange studies suggested that simulated stomatal conductance may be underestimated at night (e.g., Charusombat et al. 2010; Wu et al. 2011), and a significant loss of water through stomata can take place that may not be measured by eddy covariance systems due to low turbulence at night (Caird et al. 2007; Dawson et al. 2007; Fisher et al. 2007). Measurements of *LE* at MMSF do not indicate considerable nighttime transpiration, e.g., average nighttime *LE* varies from -2.5 to 10 W m^{-2} in the study period. Nevertheless, similar rates of eddy-covariance nighttime *LE* measured in Californian AmeriFlux sites were found to significantly underestimate nighttime transpiration as a percent of daily total when compared to sapflow-based analyses for oak-savannah (underestimation by 12 %) and *Pinus Ponderosa* (underestimation by 20 %) (Fisher et al. 2007). Even though the simulated nighttime stomatal conductance, transpiration and stomatal NH_3 flux may be underestimated in this study, the large proportion of observed nighttime relative to daytime NH_3 emission flux at MMSF (Figure 5a) suggest that other processes are also involved at night. Assuming no (or low) nighttime stomatal NH_3 emissions in this case (and no significant soil emissions – see 4.2.1), cuticular desorption could be responsible for the observed nighttime NH_3 emissions. This process is not represented in SURFATM-NH_3 that was earlier applied for modelling NH_3 fluxes of agricultural sites where cuticular adsorption is the dominant process. Emission of NH_3 from cuticles requires low cuticular resistance and that NH_3 concentrations at the leaf surface exceed those in the surrounding air. Sources of higher leaf surface NH_3 concentrations may occur from stomatal NH_3 emissions or from deposited aerosols that are converted to gaseous NH_3 at the leaf surface.

4.2.1 Leaf surface wetness and dew formation

The high solubility of NH_3 in water causes leaf surface wetness to be very important for the estimation of NH_3 fluxes. During night, radiative cooling reduces temperature, increases relative air humidity and causes dew formation. Leaf wetness caused by morning dew was found to increase the NH_3 deposition (e.g., Burkhardt et al. 2009), and there is recent evidence that dew can work as a nighttime NH_3 reservoir which is released back to the atmosphere during early morning dew evaporation (Wentworth et al. 2016). Dew formation starts when 100% relative air humidity (*RH*) is reached at the actual leaf surface which normally corresponds to about 90 % *RH* of the surrounding air (Burkhardt and Hunsche 2013). At MMSF, nighttime *RH* approaches 100 % following the rain event at night (at 1 h) on DOY 251, and *RH* increases to above 90 % throughout the following 3 nights. The largest nighttime NH_3 emissions are however seen on DOY 248–251 (Figure 5a) where *RH* is lower, e.g., it reaches maxima of 75 %, 70 % and 85 % on DOY 248–251.

In addition to morning dew formation, leaf wetness can be caused by microscopic (invisible) water films that are formed by deliquescence of hygroscopic leaf surface particles at high *RH* or as a result of transpiration (Burkhardt and Hunsche 2013). For instance, measurements of leaf surface wetness on potato over five days clearly showed two diel peaks with one leaf wetness peak being related to midday transpiration and the other leaf wetness peak being related to increasing *RH* at night (Burkhardt and Hunsche 2013). It is striking that this observed microscopic leaf wetness pattern resembles a bimodal diel curve also observed in the measured NH_3 emissions at MMSF (Figure 5a). Several studies have indicated that such microscopic water films on leaf surfaces may also enhance the emission of NH_3 depending on the concentration of dissolved ions (Sutton et al. 1998; Sutton et al. 2009; Burkhardt and Hunsche 2013; Wentworth et al. 2016). Unfortunately, we do not know how the ammonium concentrations vary overnight, however high ammonium concentration of microscopic leaf water could explain the observed nocturnal NH_3 emissions at MMSF. Theoretically, the deliquescence of aerosols happens when *RH* reaches the deliquescent relative humidity (*DRH*) which is e.g. 62 % for NH_4NO_3 particles and 80 % for $(NH_4)_2SO_4$ particles (at 298 K) (Hu et al. 2011). At *DRH*, the solid particles are transformed to larger aqueous solutions (microscopic droplets or water films) with high ion concentration. Hu et al. (2011) measured the hygroscopic growth curve for different ammonium salt particles in laboratory, and they observed gradually decreasing particle size of highly volatile particles such as NH_4NO_3 aerosols in response to increasing *RH* (below *DRH*). This led to the suggestion that small (< 50 nm) volatile ammonia particles such as NH_4NO_3 aerosols evaporate during the *RH* increasing process whereas this was not observed for the less volatile $(NH_4)_2SO_4$ particles (Hu et al. 2011). With increasing *RH* above *DRH*, the saturated solution droplets grow due to additional water condensation onto the salt solution (Hu et al. 2011), however the growth rate was less than expected for very small (< 50 nm) volatile NH_4NO_3 particles. When *RH* reaches 100 %, dew is formed. Burkhardt and Hunsche (2013) hypothesized that microscopic leaf wetness occurs on almost any plant worldwide, often permanently, and that it significantly influences the leaf surface-air exchange processes. Further studies are needed to investigate the role of *RH* on the deliquescence of deposited volatile ammonia particles and the likely occurrence of highly concentrated solutions on leaf surfaces.

4.2.2 Gaseous - aerosol phase interactions

The condensation nuclei for microscopic water typically result from deposited aerosols and may form highly concentrated solutions (Burkhardt and Hunsche 2013). Aerosol concentrations of NH_4^+ previously measured at MMSF indicated that the gaseous and aerosol phase concentrations of NH_3/NH_4^+ were of similar magnitude, but that the aerosol phase typically dominated (Hansen et al. 2015). Measured HNO_3 fluxes at MMSF showed deposition during daytime and emission during night (Hansen et al. 2015). This leads to the suggestion that the apparent nighttime HNO_3 and NH_3 emissions are caused by dissociation of aerosol NH_4NO_3 at (or near) the cool and humid leaf surfaces, and that this source of NH_3 could be responsible for the observed nighttime NH_3 emissions at MMSF. This proposed mechanism may also be related to the suggestion that increasing *RH* alters the chemical equilibrium and accelerates the evaporation of very small volatile particles such as NH_4NO_3 aerosols (Hu et al. 2011). It was also earlier suggested by Pryor et al. (2011) that NH_3 emission fluxes at MMSF could be caused by NH_4NO_3 aerosol evaporation.

4.2.3 Vapor pressure deficit and relative humidity

In the current study, we used measurement-based values for simulating ground layer and stomatal NH_3 emissions (measured at DK-Sor), and we find that these cannot explain the observed nighttime NH_3 emissions. However, the vapor pressure deficit, *VPD* (Pa) is found to be strong positively correlated with both the average nighttime *LE* (R^2 = 0.82) and the average nighttime NH_3 flux (R^2 = 0.90). The average nighttime *LE* and F_{NH3} are also strongly correlated (R^2 = 0.88) whereas *H* and F_{NH3} are not correlated (R^2 = 0.09). These relations suggest a strong association between *VPD*, *LE* and F_{NH3} at night that may be related to *VPD*-driven transpiration and foliar NH_3 emissions being supported by high ammonium concentrations at the leaf surface due to the formation of microscopic leaf wetness (by transpiration) and deliquescence of ammonia particles. In the case that NH_3 loss to the air occurs by e.g. NH_4NO_3 aerosol deliquescence and evaporation at night, the observed nighttime NH_3 emission would be strongly affected by in-canopy and leaf surface chemical reactions that are excluded in our model. In SURFATM-NH_3, the leaf surface NH_3 concentration is assumed to be zero. For further analysis, the development and application of more advanced physical and chemical models is required to represent microscopic leaf wetness (Burkhardt et al. 2013) and leaf surface NH_3 concentrations that are in equilibrium with the dissolved NH_3 concentrations at the leaf surface (Wichink Kruit et al. 2010) in order to simulate and analyze the importance of bi-directional cuticular NH_3 gaseous exchange. Model representation of inorganic chemistry interactions on the leaf surface requires many input parameters and excessive computation time, and the development of simpler empirical approaches are also needed for application in atmospheric transport models (Massad et al. 2010a; Wichink Kruit et al. 2010).

4.3 Seasonal development of the bulk NH_3 emission potentials Γ_s and Γ_g

A number of bi-directional NH_3 exchange models have been developed (e.g., Flechard et al. 2013; Nemitz et al. 2000b; Massad et al. 2010a; Sutton et al. 1995; Sutton and Fowler 1993; Wichink Kruit et al. 2010). The parameterization of seasonal dynamics during the growing season to estimate canopy NH_3 compensation point are often vastly simplified (Simpson et al. 2012), however new parameterizations are being developed for application to atmospheric transport models (Wichink Kruit et al. 2010). In practice, ecosystem (soil-vegetation) N and NH_4^+ pools are ever changing and Γ may undergo diel, seasonal and annual cycles. Modelling approaches dealing with temperature response of emission potentials should therefore theoretically also deal with temporal Γ dynamics in the various parts of an ecosystem (Flechard et al. 2013; Massad et al. 2010b; Wichink Kruit et al. 2010). Satellite observations have identified deforestation as an important source to atmospheric NH_3 (e.g., van Damme et al. 2015) and that the NH_3 emissions from large scale forest fires are important to include in atmospheric models (van Damme et al. 2014a). All these findings suggest that forest regions should be dynamically included in atmospheric models by taking into account governing processes in relation to both deposition and emission of NH_3.

Ammonia emission potentials of the ground layer (Γ_g) and stomata (Γ_s) are crucial input parameters in bi-directional NH_3 exchange models, in order to simulate the NH_3 compensation points of the ground layer and the stomata, respectively. However, realistic measurements of those are difficult and demanding to obtain and only few data exists. Wang et al. (2013) measured the pH and NH_4^+ concentration in the leaf apoplastic solution for the DK-Sor and two coniferous forest sites in order to study the seasonal variation in stomatal NH_3 compensation point. For DK-Sor, they found for the years 2008 and 2009, i.e., very close to the investigated period in this study, that χ_s peaked in the early-season during leaf expansion (6.8 µg NH_3 m^{-3}) and again in the late-season during leaf senescence (5.2 µg NH_3 m^{-3}) while in the mid-season, χ_s was lower (around 2.1 µg NH_3 m^{-3}). During leaf senescence N is translocated from the leaves into other parts of the trees leading to lower N concentrations decreasing tissue NH_4^+ concentrations especially in leaves from the canopy top (Wang et al. 2013). This pattern followed the variation in χ_s determined in parallel on the basis of the gas exchange measurements. Because of the difficulty to measure apoplastic concentrations, the significant correlation between Γ_s and the more easily measurable total foliar [NH_4^+] (Loubet et al. 2002; Mattsson et al. 2009; Wang et al. 2011) can be used to estimate Γ_s. In this study we used the seasonal measurements of Wang et al. (2011) to set Γ_s = 400 for representing a green forest canopy (MMSF) and Γ_s = 200 to represent a senescing forest canopy (DK-Sor). Apart from observed seasonal variations in Γ_s, differences in leaf N status of the two forests (2.2% for MMSF and 2.5% for DK-Sor0) support the use of different Γ_s values. To improve model simulations, this parameter should be measured for each site and maybe even parameterized with seasonal variation.

The other source for NH_3 is the ground layer (Γ_g) and particularly the decomposing litter that we described with the parameter $\Delta LPAI$. Mattsson et al. (2009) showed that the emission potential of litter could be up to 45-60 times higher than for green leaves and stems of an intensively managed grass land. Here we chose a $\Gamma_{g,min}$ value of 300, corresponding to measurements of newly fallen leaf litter at DK-Sor, and $\Gamma_{g,max}$ was estimated by trial and error method ($\Gamma_{g,max}$ = 18000). An emission potential of 18000 is high, however, in the range of values found for senescing plant material (e.g., Sutton et al. 2009; Zhang et al. 2010).

5 Conclusions

Simulations with the SURFATM-NH_3 model in combination with a canopy stomatal model show that the atmospheric NH_3 flux above a natural green forest canopy (MMSF) was dominated by the stomatal exchange (up to 50 ng NH_3-N m^{-2} s^{-1}). For a senescent canopy influenced by anthropogenic NH_3 depositions in the growing season (DK-Sor), the ground layer, or more specifically the fresh decomposing litter layer, was the largest contributor (up to 150 ng NH_3-N m^{-2} s^{-1}) to the total simulated NH_3 emissions from the forest to the atmosphere. The measured day-time pattern of the NH_3 flux for MMSF indicates a strong stomatal control by environmental factors with a strong diel signal (radiation, temperature, humidity, CO_2). However, the model underestimated the observed nighttime emissions of NH_3 for the green forest canopy (MMSF). We hypothesize that cuticular desorption is responsible for these observed NH_3 emissions at night. Recent studies found that nights with high *RH* caused morning evaporation of dew to be an important NH_3 source (Wentworth et al. 2016). In our study, nighttime NH_3 emissions were observed at nights without dew formation (e.g., higher *VPD*) and may be related to foliar NH_3 emissions induced by a combination of nighttime transpiration and deliquescence of aerosols leading to high ion concentrations of microscopic leaf surface water (Burkhardt and Hunsche 2013). Emissions of NH_3 due to microscopic leaf wetness have to our knowledge not been observed before, however, it seems likely that in-canopy gaseous-aerosol interactions may cause the formation and evaporation of aqueous aerosols and in particular microscopic leaf water at the cool and humid leaf surfaces. Atmospheric NH_3 concentrations at MMSF are consistently low which suggests that cuticular desorption may also take place during daytime where transpired water condenses on leaf surfaces (Burkhardt et al. 1999). However, further investigations including detailed process based measurements and the modelling of bidirectional cuticular NH_3 fluxes are needed in order to obtain more knowledge on this topic.

The NH_3 fluxes measured in DK-Sor showed a less pronounced diurnal pattern, however, a pattern where the flux turns from depositions to emissions parallel to the decreasing *PAI* and an increasing depth of the leaf litter layer on the forest floor comprising an important NH_3 source during leaf fall for deciduous forests. The model was not able to represent the deposition rates before leaf fall but simulated well the emission events following on leaf fall using *PAI* to scale the influence of litter on the ground layer emission potential. We conclude from this study that deciduous forests potentially comprise a natural source of NH_3 to the atmosphere, and that it is crucial to take into account the bi-directional exchange processes related to both the stomatal, cuticular and ground layer pathways in order to realistically simulate natural forest–atmosphere fluxes of NH_3. We conclude that the combination of flux measurements and modelling is a robust approach in order to understand the important, however difficult to measure all relevant processes and parameters of the NH_3 exchange with the atmosphere. More specialized studies of measurement campaigns measuring particularly the bulk ground layer emissions potential (Γ_g) as well as the potentials for the two individual ground layer contributors; the soil and the litter layer, are needed in order to obtain improved model parameterizations.

Acknowledgements

This study was supported by the ECOCLIM project funded by the Danish Strategic Research Council and the EU project ECLAIRE (project no: 282910). The CO_2 and energy flux measurements were supported by the FP 6 project NitroEurope-IP and distributed by the global flux network FLUXNET (http://fluxnet.ornl.gov/). Additionally, a travel grant from The Danish Agency for Science, Technology and Innovation to Kristina Hansen has supported this study financially. The authors gratefully acknowledge Tyler Roman, Edward Brzostek, and Rich Phillips (Indiana University) for providing meteorological and biological data from the MMSF site.

Appendix A

Description of the two-layer bi-directional NH_3 model

The two-layer bi-directional NH_3 exchange model simulates the total net atmospheric NH_3 flux (F_T; ng m^{-2} s^{-1}) as a sum of each of the forest component fluxes; the stomatal NH_3 flux (F_s; ng m^{-2} s^{-1}), the cuticular NH_3 flux (F_w; ng m^{-2} s^{-1}) and the ground NH_3 flux (F_g; ng m^{-2} s^{-1}) which are all related to the NH_3 canopy compensation point (χ_c; ng m^{-3}) (Nemitz et al. 2000b):

$$\chi_c = \frac{\chi_a (r_a r_b)^{-1} + \chi_s (r_a r_s)^{-1} + (r_b r_s)^{-1} + (r_g r_s)^{-1} + \chi_g (r_b r_g)^{-1}}{(r_a r_b)^{-1} + (r_a r_s)^{-1} + (r_a r_w)^{-1} + (r_b r_g)^{-1} + (r_b r_s)^{-1} + (r_b r_w)^{-1} + (r_g r_s)^{-1} + (r_g r_w)^{-1}} \quad \text{(A1)}$$

$$F_s = -\frac{\chi_c - \chi_s}{r_s} \quad \text{(A2)}$$

$$F_w = -\frac{\chi_c}{r_w} \quad \text{(A3)}$$

$$F_g = -\frac{\chi_c - \chi_g}{r_g} \quad \text{(A4)}$$

where r_a (s m^{-1}) is the aerodynamic resistance of the canopy, r_b (s m^{-1}) is the quasi-laminar boundary layer resistance of the canopy, r_s (s m^{-1}) is the stomatal resistance, r_w (s m^{-1}) is the cuticular resistance, r_g (s m^{-1}) is the ground layer resistance which represents a series of the in-canopy aerodynamic resistance and the quasi laminar boundary-layer resistance of the ground layer (Nemitz et al. 2001). χ_g and χ_s (ng m^{-3}) are the ground layer compensation point and the stomatal NH_3 compensation points, respectively.

Appendix B

Description of the coupled photosynthesis-stomatal conductance model

The coupled leaf photosynthesis and stomatal resistance model (Collatz et al. 1991) was parameterized for the specific forest sites using measured plant area index, *PAI* (m^2 m^{-2}) as a proxy of the leaf area index (*LAI*). The model uses input data of the air temperature, T_a (°C), soil temperature, T_s (°C), leaf temperature, T_L (°C), relative humidity, *RH* (%), photosynthetic active radiation, *PAR* (W m^{-2}), sensible heat flux, H (W m^{-2}), wind speed, u (m s^{-1}), friction velocity, u_* (m s^{-1}), and *PAI* (m^2 m^{-2}), to simulate the stomatal conductance, g_s (m s^{-1}) and the leaf photosynthesis (or net carbon assimilation), A_n (μmol m^{-2} s^{-1}), in an iterative setup (Figure 9). A_n is estimated as the minimum of three potential capacities and the leaf dark respiration, R_D (μmol m^{-2} s^{-1}), (Collatz et al. 1991, Farquhar et al. 1980b) :

$$A_n = \min\{J_E, J_C, J_S\} - R_D \quad \text{(B1)}$$

J_E is the light-limited assimilation rate (μmol m^{-2} s^{-1}), J_C is the rubisco-limited assimilation rate (μmol m^{-2} s^{-1}), and J_S is the assimilation rate due to the limitation of the export of assimilates inside the leaf (μmol m^{-2} s^{-1}) simulated as (Collatz et al. 1991):

$$J_E = a\,\alpha\,Q\,\frac{C_i - \Gamma^*}{C_i + 2\Gamma^*} \quad \text{(B2)}$$

$$J_C = \frac{V_{c,max}\,(C_i - \Gamma^*)}{C_i + K_c\left(1 + \frac{O_2}{K_0}\right)} \quad \text{(B3)}$$

$$J_S = 0.5V_{c,max} \quad \text{(B4)}$$

where a is the leaf absorptivity of *PAR*, α (μmol m^{-2} s^{-1}) is the maximum quantum yield,

Q is *PAR*, C_i (Pa) is the internal CO_2 pressure, Γ_* (Pa) is the CO_2 compensation point, $V_{c,max}$ (μmol m^{-2} s^{-1}) is the maximum carboxylation rate of Rubisco, O_2 is the oxygen intercellular partial pressure (Pa), and K_C (40.4 Pa) and K_O (24,800 Pa) are the Michaelis constant for CO_2 fixation and oxygen inhibition, respectively. R_D can experimentally be determined by gas exchange measurements of leaves, but here it is determined by a fraction of $V_{c,max}$ following Collatz et al. (1991):

$$R_D = 0.015V_{c,max} \quad \text{(B5)}$$

The stomatal conductance is simulated following Ball et al. (1987):

$$g_s = m\,\frac{A_n\,h_s}{C_s} + b \quad \text{(B6)}$$

where h_s (%) is the relative humidity at the leaf surface, C_s (Pa) is the CO_2 partial pressure on the leaf surface, and m = 7 and b = 0.01 mol m^{-2} s^{-1} are constants.

The leaf temperature, T_L (°C), is simulated as:

$$T_L = \frac{H\,r_{abh}}{\rho\,c_p} + T_a \quad \text{(B7)}$$

where r_{abh} (s m^{-1}) is the total resistance to heat, ρ (kg m^{-3}) is the air density, and c_p is the specific heat for air at constant pressure (J kg^{-1} K^{-1}).

$V_{c,max}$ is strongly dependent on the availability of leaf nitrogen and leaf temperature. Hence it is expected that $V_{c,max}$ at 25 ° C is higher for the DK-Sor site than for the MMSF site, since the DK-Sor site is located in an agricultural region exposed to large NH_3 deposition (Skiba et al. 2009). The applied parameter values for $V_{c,max,}$ at 25 ° C for DK-Sor ($100 \cdot 10^{-6}$ mol m^{-2} s^{-1}) and MMSF ($70 \cdot 10^{-6}$ mol m^{-2} s^{-1}) are within the range of values found and used for this plant functional type (PFT) in other terrestrial biosphere models (Kattge et al. 2009; Rogers 2014). Three different parameterizations of the soil and ecosystem respiration were furthermore tested in order to obtain the best representation; two of them based on the temperature-controlled soil (R_s) or ecosystem (R_{eco}) respiration model from Lloyd and Taylor (1994) and one total ecosystem respiration (*TER*) parameterized for DK-Sor by Wu et al. (2012):

$$R_s = R_{10} \times \exp\left(308.56 - \left(\frac{1}{T_{ref} - T_0} - \frac{1}{T_s - T_0}\right)\right) \quad \text{(B8)}$$

$$R_{eco} = R_{eco,ref} \times \exp\left(308.56 - \left(\frac{1}{T_{ref} - T_0} - \frac{1}{T_a - T_0}\right)\right) \quad \text{(B9)}$$

$$TER = R_{eco,ref}\, Q_{10}^{\frac{T_s - T_0}{10}} \quad \text{(B10)}$$

where R_{10} (µmol m^{-2} s^{-1}) is the soil respiration at 10°C, T_s (°C) is soil temperature, T_{ref} (°C) is the reference temperature set to 10°C as in the original model, T_0 (°C) is a regression constant of -46.02°C (Lloyd and Taylor 1994), T_{air} (°C) is the ambient air temperature, $R_{eco,ref}$ (µmol m^{-2} s^{-1}) is the respiration at T_{ref} estimated from nighttime data, and Q_{10} is the temperature sensitivity parameter and set to a constant value of 2. The parameterization of *TER* by Wu et al. (2012) was used for DK-Sor, and the general parameterization (R_{eco}) was used for MMSF.

Subtracting the simulated soil respiration (R_s) from A_c (canopy net photosynthesis per ground area) being A_n (leaf net photosynthesis per leaf area) upscaled to the canopy scale using *LAI* as proposed by Sellers et al. (1992), the net CO_2 exchange was calculated at canopy scale ($NEE = -A_c + R_s$) and can be directly tested with eddy covariance CO_2 flux measurements (Pilegaard et al. 2011).

References

Allen, R.G., Pereira, L.S., Raes, D., Smith, M., 1998. Crop evapotranspiration: Guidelines for computing crop requirements. FAO Irrigation and Drainage Paper No. 56, FAO, Rome.

Andersen, H.V., Hovmand, M.F., Hummelshøj, P., Jensen, N.O., 1999. Measurements of ammonia concentrations, fluxes and dry deposition velocities to a spruce forest 1991–1995. Atmos. Environ. 33, 1367–1383. http://dx.doi.org/10.1016/S1352-2310(98)00363-X.

Andreae, M. and Merlet, P., 2001. Emission of trace gases and aerosols from biomass burning. Global Biogeochem. Cycles 15, 955-966. http://dx.doi.org/10.1029/2000GB001382.

Ball, J., Woodrow, I., Berry, J., 1987. A model predicting stomatal conductance and its contribution to the control of photosynthesis under different environmental conditions, in: Progress in photosynthesis research, Biggins, I. (Ed.), Martinus Nijhoff Publishers, Amsterdam, 221-224. ISBN: 978-94-017-0521-9.

Bash, J.O., Cooter, E.J., Dennis, R.L., Walker, J.T., Pleim, J.E., 2013. Evaluation of a regional air-quality model with bidirectional NH_3 exchange coupled to an agroecosystem model. Biogeosciences 10, 1635-1645. http://dx.doi.org/10.5194/bg-10-1635-2013.

Bates, R.G. and Pinching, G.D., 1950. Dissociation Constant of Aqueous Ammonia at 0 to 50° from E. m. f. Studies of the Ammonium Salt of a Weak Acid. J. Am. Chem. Soc. 72 (3), pp 1393–1396. http://dx.doi.org/10.1021/ja01159a087.

Burkhardt, J., Kaiser, H., Goldbach, H., Kappen, L, 1999. Measurements of electrical leaf surface conductance reveal recondensation of transpired water vapour on leaf surfaces. Plant, Cell and Environment 22, 189-196. http://dx.doi.org/10.1046/j.1365-3040.1999.00387.x.

Burkhardt, J., Flechard, C.R., Gresens, F., Mattson, M., Jongejan, P.A.C., Erisman, J.W., Weidinger, T., Meszaros, R., Nemitz, E., Sutton, M.A., 2009. Modelling the chemical interactions of atmospheric ammonia with leaf surface wetness in a managed grassland canopy. Biogeosciences 6, 67-84. http://dx.doi.org/10.5194/bg-6-67-2009.

Burkhardt, J. and Hunsche, M., 2013. “Breath figures” on leaf surfaces formation and effects of microscopic leaf wetness, Frontiers in Plant Science, 4, 422, 1-9. http://dx.doi.org/10.3389/fpls.2013.00422.

Businger, J.A. and Oncley, S.P., 1990. Flux measurement with conditional sampling. J. Atmos. Ocean. Technol. 7, 349-352. http://dx.doi.org/10.1175/1520-0426(1990)007<0349:FMWCS>2.0.CO;2.

Caird, M.A., Richards, J.H., Donovan, L.A., 2007. Nighttime stomatal conductance and transpiration in C_3 and C_4 plants. Plant Physiology 143, 4-10. http://dx.doi.org/10.1104/pp.106.092940.

Callesen, I., Nilsson, L.O., Schmidt, I.K., Vesterdal, L., Ambus, P., Christiansen, J.R., Högberg, P., Gundersen, P., 2013. The natural abundance of ^{15}N in litter and soil profiles under six temperatue tree species: N cycling depends on tree species trait and site fertility. Plant Soil 368, 375-392. http://dx.doi.org/10.1007/s11104-012-1515-x.

Carslaw, K.S., Boucher, O., Spracklen, D.V., Mann, G.W., Rae, J.G.L., Woodward, S., Kulmala, M., 2010. A review of natural aerosol interactions and feedbacks within the Earth system. Atmos. Chem. Phys. 10, 1701-1737. http://dx.doi.org/ 10.5194/acp-10-1701-2010.

Charusombat, U., Niyogi, D., Kumar, A., Wang, H., Chen, F., Guenther, A.B., Turnipseed, A.A., Alapaty, K., 2010. Evaluating a new deposition velocity module in the Noah land surface model. Bound-Lay Meteorol 137, 271-290. http://dx.doi.org/10.1007/s10546-010-9531-y.

Collatz, G., Ball, J., Grivet, C., Berry, J., 1991. Physiological and environmental-regulation of stomatal conductance, photosynthesis and transpiration - a model that includes a laminar boundary-layer. Agric. For. Meteorol. 54, 107-136. http://dx.doi.org/10.1016/0168-1923(91)90002-8.

David, M., Loubet, B., Cellier, P., Mattsson, M., Schjoerring, J.K., Nemitz, E., Roche, R., Riedo, M., Sutton, M. A., 2009. Ammonia sources and sinks in an intensively managed grassland canopy. Biogeosciences 6, 1903-1915. http://dx.doi.org/10.5194/bg-6-1903-2009.

Dawson, T.E., Burgess, S.S.O., Tu, K.P., Oliveira, R.S., Santiago, L.S., Fisher, J.B., Simonin, D.A., Ambrose, A.R., 2007. Nighttime transpiration in woody plants from contrasting ecosystems. Tree Physiology 27, 561-575. http://dx.doi.org/10.1093/treephys/27.4.561.

Erisman, J.W. and Wyers, G.P., 1993. Continuous measurements of surface exchange of SO_2 and NH_3 - Implications for their possible interaction in the deposition process. Atmos. Environ. Part A. 27, 1937-1949. http://dx.doi.org/10.1016/0960-1686(93)90266-2.

Farquhar, G., Firth, P., Wetselaar, R., Weir, B., 1980a. On the gaseous exchange of ammonia between leaves and the environment - Determination of the ammonia compensation point. Plant Physiol. 66, 710-714. http://dx.doi.org/doi: 10.1104/pp.66.4.710.

Farquhar, G., Caemmerer, S., Berry, J., 1980b. A biochemical model of photosynthetic CO_2 assimilation in leaves of C_3 species. Planta 149, 78-90. http://dx.doi.org/ 10.1007/BF00386231.

Ferrara, R.M., Loubet, B., Decuq, C., Palumbo, A.D., Di Tommasi, P., Magliulo, V., Masson, S., Personne, E., Cellier, P., Rana, G., 2014. Ammonia volatilisation following urea fertilisation in an irrigated sorghum crop in Italy. Agric. For. Meteorol. 195, 179-191. http://dx.doi.org/10.1016/j.agrformet.2014.05.010.

Ferrara, R.M., Carozzib, M., Di Tommasi, P., Nelsond, D.D., Fratinie, G., Bertolinif, T., Magliuloc, V., Acutisg, M., Ranaa, G., 2016. Dynamics of ammonia volatilisation measured by eddy covariance during slurry spreading in north Italy. Agriculture, Ecosystems & Environment 219, 1–13. http://dx.doi.org/doi:10.1016/j.agee.2015.12.002.

Fisher, J.B., Baldochi, D.D., Misson, L., Dawson, T.E., Goldstein, A.H., 2007. What the towers don't see at night: nocturnal sap flow in trees and shrubs at two AmeriFlux sites in California. Tree Physiology 27, 597-610. http://dx.doi.org/10.1093/treephys/27.4.597.

Flechard, C.R., Massad, R., Loubet, B., Personne, E., Simpson, D., Bash, J.O., Cooter, E.J., Nemitz, E., Sutton, M.A., 2013. Advances in understanding, models and parameterizations of biosphere-atmosphere ammonia exchange. Biogeosciences 10, 5183-5225. http://dx.doi.org/10.5194/bg-10-5183-2013.

Gessler, A., Rienks, M., Rennenberg, H., 2000. NH_3 and NO_2 fluxes between beech trees and the atmosphere – correlation with climatic and physiological parameters. New Phytol. 147, 539-560. http://dx.doi.org/10.1046/j.1469-8137.2000.00712.x.

Greenberg, J.P., Asensio, D., Turnipseed, A., Guenther, A.B., Karl, T., Gochis, D., 2012. Contribution of leaf and needle litter to whole ecosystem BVOC fluxes. Atmos. Environ. 59, 302-311. http://dx.doi.org/10.1016/j.atmosenv.2012.04.038.

Hamaoui-Laguel, L, Meleux, F., Beekmann, M., Bessagnet, B., Génermont, S., Cellier, P., and Létinois, L., 2014. Improving ammonia emissions in air quality modelling for France. Atmos. Environ. 92, 584-595. http://dx.doi.org/10.1016/j.atmosenv.2012.08.002.

Hansen, K., Sørensen, L.L., Hertel, O., Geels, C., Skjøth, C.A., Jensen, B., Boegh, E., 2013. Ammonia emissions from deciduous forest after leaf fall. Biogeosciences 10, 4577-4589. http://dx.doi.org/10.5194/bg-10-4577-2013.

Hansen, K., Pryor, S.C., Boegh, E., Hornsby, K.E., Sørensen, L.L., 2015. Background concentrations and fluxes of atmospheric ammonia over a deciduous forest. Agric. For. Meteorol. 214-215, 380-392. http://dx.doi.org/10.1016/j.agrformet.2015.09.004.

Hendriks, C., Kranenburg, R., Kuenen, J., van Gijlswijk, R., Wichink Kruit, R.J., Segers, A., Denier van der Gon, H., Schaap, M., 2013. The origin of ambient Particulate Matter concentrations in the Netherlands. Atmos. Environ. 69, 289–303. http://dx.doi.org/10.1016/j.atmosenv.2012.12.017.

Hertel, O., Skjøth, C.A., Reis, S., Bleeker, A., Harrison, R.M., Cape, J.N., Fowler, D., Skiba, U., Simpson, D., Jickells, T., Kulmala, M., Gyldenkærne, S., Sørensen, L.L., Erisman, J.W., Sutton, M.A., 2012. Governing processes for reactive nitrogen compounds in the European atmosphere. Biogeosciences 9, 4921-4954. http://dx.doi.org/10.5194/bg-9-4921-2012.

Hu, D., Chen, J., Ye, X, Li, L., Yang, X., 2011. Hygroscopicity and evaporation of ammonium chloride and ammonium nitrate: Relative humidity and size effects on the growth factor. Atmos. Environ. 45, 2349-2355. http://dx.doi.org/10.1016/j.atmosenv.2011.02.024.

Husted, S. and Schjoerring, J.K., 1996. Ammonia flux between oilseed rape plants and the atmosphere in response to changes in leaf temperature, light intensity, and air humidity. Plant Physiol. 112, 67–74. http://dx.doi.org/10.1104/pp.112.1.67.

Kattge, J., Knorr, W., Raddatz, T., Wirth, C., 2009. Quantifying photosynthetic capacity and its relationship to leaf nitrogen content for global-scale terrestrial biosphere models. Glob. Change Biol. 15, 976–991. http://dx.doi.org/10.1111/j.1365-2486.2008.01744.x.

Kuenen, J.J.P., Visschedijk, A.J.H., Jozwicka, M., Denier van der Gon, H.A.C., 2014. TNO-MACC_II emission inventory; a multi-year (2003–2009) consistent high-resolution European emission inventory for air quality modelling. Atmos. Chem. Phys. 14, 10963–10976. http://dx.doi.org/10.5194/acp-14-10963-2014.

Langford, A.O. and Fehsenfeld, F.C., 1992. Natural vegetation as a source or sink for atmospheric ammonia: A case study. Science 255, 581-583. http://dx.doi.org/10.1126/science.255.5044.581.

Lloyd, J. and Taylor, J., 1994. On the temperature dependence of soil respiration. Funct. Ecol. 8, 315-323. http://dx.doi.org/ 10.2307/2389824.

Loubet, B., Milford, C., Hill, P., Tang, Y., Cellier, P., Sutton, M., 2002. Seasonal variability of apoplastic NH_4^+ and pH in an intensively managed grassland. Plant Soil 238, 97-110. http://dx.doi.org/10.1023/A:1014208926195.

Loubet, B., Decuq, C., Personne, E., Massad, R.S., Flechard, C., Fanucci, O., Mascher, N., Gueudet, J.-C., Masson, S., Durand, B., Genermont, S., Fauvel, Y., Cellier, P., 2012. Investigating the stomatal, cuticular and soil ammonia fluxes over a growing tritical crop under high acidic loads. Biogeosciences 9, 1537-1552. http://dx.doi.org/10.5194/bg-9-1537-2012.

Madsen, H.B., Holst, K.A., 1988. A nation-wide mapping of dry soils for plant production – A case study from Denmark. Geografisk Tidsskrift 88: 1-9. Available at https://tidsskrift.dk/index.php/geografisktidsskrift/article/view/5426/10274

Massad, R.-S., Tuzet, A., Loubet, B., Perrier, A., Cellier, P., 2010a. Model of stomatal ammonia compensation point (STAMP) in relation to the plant nitrogen and carbon metabolisms and environmental conditions. Ecol. Model. 221, 479–494. http://dx.doi.org/10.1016/j.ecolmodel.2009.10.029.

Massad, R.S., Nemitz, E., Sutton, M.A., 2010b. Review and parameterisation of bi-directional ammonia exchange between vegetation and the atmosphere. Atmos. Chem. and Phys. 10, 10359-10386. http://dx.doi.org/10.5194/acp-10-10359-2010.

Mattsson, M., Hausler, R.E., Leegood, R.C., Lea, P.J., Schjoerring, J.K., 1997. Leaf-atmosphere NH_3 exchange in barley mutants with reduced activities of glutamine synthetase. Plant Physiol. 114, 1307–1312. http://dx.doi.org/10.1104/pp.114.4.1307.

Mattsson, M., Herrmann, B., David, M., Loubet, B., Riedo, M., Theobald, M.R., Sutton, M.A., Bruhn, D., Neftel, A., Schjoerring, J.K., 2009. Temporal variability in bioassays of the stomatal ammonia compensation point in relation to plant and soil nitrogen parameters in intensively managed grassland. Biogeosciences 6, 171-179. http://dx.doi.org/10.5194/bg-6-171-2009.

Monteith, J.L. and Unsworth, M.H., 1990. Principles of Environmental Physics. Edward Arnold, Sevenoaks, 2nd edition, pp. xii + 291.

Muller, R.N., 2003. Nutrient relations of the herbaceous layer in deciduous forest ecosystems, pages 15–37 in Gilliam, F.S. and M.R. Roberts, editors. eds. The Herbaceous Layer in Forests of Eastern North America. New York Oxford University Press.

Nemitz, E., Sutton, M., Gut, A., San Jose, R., Husted, S., Schjoerring, J., 2000a. Sources and sinks of ammonia within an oilseed rape canopy. Agric. For. Meteorol. 105, 385-404. http://dx.doi.org/10.1016/S0168-1923(00)00205-7.

Nemitz, E., Sutton, M., Schjoerring, J., Husted, S., Wyers, G., 2000b. Resistance modelling of ammonia exchange over oilseed rape. Agric. For. Meteorol. 105, 405-425. http://dx.doi.org/10.1016/S0168-1923(00)00206-9.

Nemitz, E., Milford, C., Sutton, M.A., 2001. A two-layer canopy compensation point model for describing bi-directional biosphere-atmosphere exchange of ammonia. Q. J. R. Meteorol. Soc. 127, 815-833. http://dx.doi.org/10.1002/qj.49712757306.

Papale, D., Reichstein, M., Aubinet, M., Canfora, E., Bernhofer, C., Kutsch, W., Longdoz, B., Rambal, S., Valentini, R., Vesala, T., Yakir, D., 2006. Towards a standardized processing of Net Ecosystem Exchange measured with eddy covariance technique: algorithms and uncertainty estimation. Biogeosciences 3, 571-583. http://dx.doi.org/10.5194/bg-3-571-2006.

Paulot, F., Jacob, D.J., Pinder, R.W., Bash, J.O., Travis, K., Henze, D.K., 2014. Ammonia emissions in the United States, European Union, and China derived by high-resolution inversion of ammonium wet deposition data: Interpretation with a new agricultural emissions inventory (MASAGE_NH3). J. Geophys. Res. Atmos. 119, 4343-4364. http://dx.doi.org/10.1002/2013JD021130.

Personne, E., Loubet, B., Herrmann, B., Mattsson, M., Schjoerring, J.K., Nemitz, E., Sutton, M.A., Cellier, P., 2009. SURFATM-NH3: a model combining the surface energy balance and bi-directional exchanges of ammonia applied at the field scale, Biogeosciences, 6, 1371-1388. http://dx.doi.org/10.5194/bg-6-1371-2009.

Personne, E., Tardy, F., Génermont, S., Decuq, C., Gueudet, J.-C., Maschera, N., Durand, B., Masson, S., Lauransot, M., Fléchard, C., Burkhardt, J., Loubet, B., 2015. Investigating sources and sinks for ammonia exchanges between the atmosphere and a wheat canopy following slurry application with trailing hose. Agric. For. Meteorol. 207, 11-23. http://dx.doi.org/10.1016/j.agrformet.2015.03.002.

Pilegaard, K., Ibrom, A., Courtney, M.S., Hummelshøj, P., Jensen, N.O., 2011. Increasing net CO_2 uptake by a Danish beech forest during the period from 1996 to 2009. Agric. For. Meteorol. 151, 934-946. http://dx.doi.org/10.1016/j.agrformet.2011.02.013.

Pinder, R.W., Gilliland, A. B., Dennis, R.L., 2008. Environmental impact of atmospheric NH_3 emissions under present and future conditions in the eastern United States. Geophys. Res. Lett. 35, L12808. http://dx.doi.org/10.1029/2008GL033732.

Pouliot, G., Pierce, T., van der Gon, H.D., Schaap, M., Moran, M., Nopmongcol, U., 2012. Comparing emission inventories and model-ready emission datasets between Europe and North America for the AQMEII project. Atmos. Environ. 53, 4-14. http://dx.doi.org/10.1016/j.atmosenv.2011.12.041.

Pryor, S.C., Barthelmie, R.J., Sørensen, L.L., Jensen, B., 2001. Ammonia concentrations and fluxes over a forest in the midwestern USA. Atmos. Environ. 35, 5645–5656. http://dx.doi.org/10.1016/S1352-2310(01)00259-x.

Pryor, S.C., Barthelmie, R.J., Sørensen, L.L., McGrath, J.G., Hopke, P., Petaja, T., 2011. Spatial and vertical extent of nucleation events in the Midwestern USA: insights from the Nucleation In ForesTs (NIFTy) experiment. Atmos. Chem. Phys. 11, 1641–1657, http://dx.doi.org/10.5194/acp-11-1641-2011.

Rao, S.T., Galmarini, S., Puckett, K., 2011. Air Quality Model Evaluation International Initiative (AQMEII) advancing the state of the science in regional photochemical modeling and its applications. Bull. Am. Meteorol. Soc. 92, 23-30. http://dx.doi.org/10.1175/2010BAMS3069.1.

Reichstein, M., Falge, E., Baldocchi, D., Papale, D., Aubinet, M., Berbigier, P., Bernhofer, C., Buchmann, N., Gilmanov, T., Granier, A., Grunwald, T., Havrankova, K., Ilvesniemi, H., Janous, D., Knohl, A., Laurila, T., Lohila, A., Loustau, D., Matteucci, G., Meyers, T., Miglietta, F., Ourcival, J., Pumpanen, J., Rambal, S., Rotenberg, E., Sanz, M., Tenhunen, J., Seufert, G., Vaccari, F., Vesala, T., Yakir, D., Valentini, R., 2005. On the separation of net ecosystem exchange into assimilation and ecosystem respiration: review and improved algorithm. Global Change Biol. 11, 1424-1439. http://dx.doi.org/10.1111/j.1365-2486.2005.001002.x.

Reis, S., Pinder, R.W., Zhang, M., Lijie, G., Sutton, M.A., 2009. Reactive nitrogen in atmospheric emission inventories. Atmos. Chem. Phys. 9, 7657-7677. http://dx.doi.org/10.5194/acp-9-7657-2009.

Riddick, S.N., Blackall, T.D., Dragosits, U., Daunt, F., Braban, C.F., Tang, Y.S., MacFarlane, W., Taylor, S., Wanless, S., Sutton, M.A., 2014. Measurement of ammonia emissions from tropical seabird colonies. Atmos. Environ. 89, 35-42. http://dx.doi. org/10.1016/j.atmosenv.2014.02.012.

Rogers, A., 2014. The use and misuse of $V_{c,max}$ in earth system models. Photosynth. Res. 119, 15–29. http://dx.doi.org/10.1007/s11120-013-9818-1.

Schjoerring, J.K., Husted, S., Mattsson, M., 1998. Physiological parameters controlling plant-atmosphere ammonia exchange. Atmos. Environ. 32, 491-498. http://dx.doi. org/10.1016/S1352-2310(97)00006-X.

Schmid, H.P., Grimmond, C.S.B., Cropley, F., Offerle, B., Su, H.-B., 2000. Measurements of CO_2 and energy fluxes over a mixed hardwood forest in the mid-western United States. Agric. For. Meteorol. 103, 357-374. http://dx.doi.org/10.1016/S0168-1923(00)00140-4.

Sellers, P., Berry, J., Collatz, G., Field, C., Hall, F., 1992. Canopy reflectance, photosynthesis, and transpiration. III. A reanalysis using improved leaf models and a new canopy intergration scheme. Remote Sens. Environ. 42, 187-216. http://dx.doi.org/10.1016/0034-4257(92)90102-P.

Simpson, D., Benedictow, A., Berge, H., Bergström, R., Emberson, L.D., Fagerli, H., Flechard, C.R., Hayman, G.D., Gauss, M., Jonson, J.E., Jenkin, M.E., Nyíri, A., Richter, C., Semeena, V.S., Tsyro, S., Tuovinen, J.-P., Valdebenito, Á., Wind, P., 2012. The EMEP MSC-W chemical transport model – technical description. Atmos. Chem. Phys. 12, 7825-7865. http://dx.doi.org/10.5194/acp-12-7825-2012.

Skjøth, C.A. and Geels, C., 2013. The effect of climate and climate change on ammonia emissions in Europe. Atmos. Chem. Phys. 13, 117-128. http://dx.doi.org/ 10.5194/acp-13-117-2013.

Skjøth, C.A., Geels, C., Berge, H., Gyldenkaerne, S., Fagerli, H., Ellermann, T., Frohn, L.M., Christensen, J., Hansen, K.M., Hansen, K., Hertel, O., 2011. Spatial and temporal variations in ammonia emissions - a freely accessible model code for Europe. Atmos. Chem. Phys. 11, 5221-5236. http://dx.doi.org/10.5194/acp-11-5221-2011.

Skiba, U., Jones, S.K., Drewer, J., Tang, Y.S., van Dijk, N., Helfner, C., Nemitz, E., Twigg, M., Famulari, D., Owen, S., Pihlatie, M., Vesala, T., Larsen, K.S., Carter, M.S., Ambus, P., Ibrom, A., Beier, C., Hensen, A., Frumau, A., Brüggemann, N., Gasche, R., Neftel, A., Spirig, C., Horvath, L., Freibauer, A., Cellier, P., Laville, P., Loubet, B., Magliulo, E., Bertolini, T., Suefert, G., Anderson, M., Manca, G., Laurila, T., Aurela, A., Zechmeister-Boltenstern, S., Kitzler, B., Schaufler, G., Siemens, J., Kindler, R., Flechard, C., Sutton, M.A., 2009. Biosphere atmosphere exchange of reactive nitrogen and greenhouse gases at the NitroEurope core flux measurement sites: Measurement strategy and first annual data sets. Agriculture, Ecosystems and Environment 133, 139-149. http://dx.doi.org/10.1016/j.agee.2009.05.018.

Stoy, P.C., Mauder, M., Foken, T., Marcolla, B., Boegh, E., Ibrom, A., Arain, M.A., Arneth, A., Aurela, M. Bernhofer, C., Cescatti, A., Dellwik, E., Duce, P., Gianelle, D., van Gorsel, E., Kiely, G., Knohl, A., Margolis, H., McCaughey, H., Merbold, L., Montagnani, L., Papale, D., Reichstein, M., Serrano-Ortiz, P., Sottocornola, M., Saunders, M., Spano, D., Vaccari, F., Varlagin, A., 2013. A data-driven analysis of energy balance closure across FLUXNET research sites: The role of landscape-scale heterogeneity. Agric. For. Meteorol. 171-172, 137-152. http://dx.doi.org/10.1016/j.agrformet.2012.11.004.

Sørensen, L.L., Granby, K., Nielsen, H., Asman, W.A.H., 1994. Diffusion scrubber technique used for measurements of atmospheric ammonia. Atmos. Environ. 28, 3637-3645. http://dx.doi.org/10.1016/1352-2310(94)00189-R.

Sørensen, L., Hertel, O., Skjøth, C., Lund, M., Pedersen, B., 2003. Fluxes of ammonia in the coastal marine boundary layer. Atmos. Environ. 37, S167-S177. http://dx.doi.org/10.1016/S1352-2310(03)00247-4.

Sutton, M. and Fowler, D., 1993. A canopy model for inferrring bi-directional plant-atmosphere exchange of ammonia. Proc 6th. European symposium on physicochemical behaviour of atmospheric pollutants Varese, Italy, Italy, pp. 601-608.

Sutton, M., Schørring, J.K., Wyers, G.P., 1995. Plant-atmosphere exchange of ammonia. Philos. Trans. R. Soc. London, Ser. A. http://dx.doi.org/10.1098/rsta.1995.0033.

Sutton, M.A., Perthue, E., Fowler, D., Storeton-West, R.L., Cape, J.N., Arends, G.G., Mols, J.J., 1997. Vertical distribution and fluxes of ammonia at Great Dun Fell. Atmos. Environ. 31, 2615–2624. http://dx.doi.org/10.1016/S1352-2310(96)00180-X.

Sutton, M.A., Burkhardt, J.K., Guerin, D., Nemitz, E., Fowler, D., 1998. Development of resistance models to describe measurements of bi-directional ammonia surface-atmosphere exchange Atmos. Environ. 32, 473-480. http://dx.doi.org/10.1016/S1352-2310(97)00164-7.

Sutton, M.A., Nemitz, E., Milford, C., Campbell, C., Erisman, J.W., Hensen, A., Cellier, P., David, M., Loubet, B., Personne, E., Schjoerring, J.K., Mattsson, M., Dorsey, J.R., Gallagher, M.W., Horvath, L., Weidinger, T., Meszaros, R., Dämmgen, U., Neftel, A., Herrmann, B., Lehman, B.E., Flechard, C.,Burkhardt, J., 2009. Dynamics of ammonia exchange with cut grassland: synthesis of results and conclusions of the GRAMINAE Integrated Experiment. Biogeosciences 6, 2907-2934. http://dx.doi.org/10.5194/bg-6-2907-2009.

Sutton, M.A., Oenema, O., Erisman, J.W., Leip, A., van Grinsven, H., Winiwarter, W., 2011. Too much of a good thing. Nature 472, 159-161. http://dx.doi.org/10.1038/472159a.

Sutton, M.A., Reis, S., Riddick, S.N., Dragosits, U., Nemitz, E., Theobald, M.R., Tang, Y.S., Braban, C.F., Vieno, M., Dore, A.J., Mitchell, R.F., Wanless, S., Daunt, F., Fowler, D., Blackall, T.D., Milford, C., Flechard, C.R., Loubet, B., Massad, R., Cellier, P., Personne, E., Coheur, P.F., Clarisse, L., Van Damme, M., Ngadi, Y., Clerbaux, C., Skjøth, C.A., Geels, C., Hertel, O., Wichink Kruit, R.J., Pinder, R.W., Bash, J.O., Walker, J.T., Simpson, D., Horvath, L., Misselbrook, T.H., Bleeker, A., Dentener, F., de Vries, W., 2013. Towards a climate-dependent paradigm of ammonia emission and deposition. Philos. Trans. R. Soc. London, Ser. B. 368. http://dx.doi.org/10.1098/rstb.2013.0166.

Theobald, M., Crittenden, P., Hunt, A., Tang, Y., Dragosits, U., Sutton, M., 2006. Ammonia emissions from a Cape fur seal colony, Cape Cross, Namibia. Geophys. Res. Lett. 33, L03812. http://dx.doi.org/10.1029/2005GL024384.

Thompson, S.E., Harman, C.J., Konings, A.G., Sivapalan, M., Neal, A., Troch, P.A., 2011. Comparative hydrology across AmeriFlux sites: The variable roles of climate, vegetation, and groundwater. Water Resour. Res. 47, W00J07. http://dx.doi.org/ 10.1029/2010WR009797.

Tuccella, P., Curci, G., Visconti, G., Bessagnet, B., Menut, L., Park, R.J., 2012. Modeling of gas and aerosol with WRF/Chem over Europe: Evaluation and sensitivity study. J. Geophys. Res. Atmos. 117, D03303. http://dx.doi.org/10.1029/2011JD016302.

Van Damme, M., Clarisse, L., Heald, C.L., Hurtmans, D., Ngadi, Y., Clerbaux, C., Dolman, A.J., Erisman, J.W., Coheur, P.F., 2014a. Global distributions, time series and error characterization of atmospheric ammonia (NH_3) from IASI satellite observations. Atmos. Chem. Phys. 14, 2905-2922. http://dx.doi.org/10.5194/acp-14-2905-2014.

Van Damme, M., Wichink Kruit, R.J., Schaap, M., Clarisse, L., Clerbaux, C., Coheur, P.-F., Dammers, E., Dolman, A.J., Erisman, J.W., 2014b. Evaluating 4 years of atmospheric ammonia (NH_3) over Europe using IASI satellite observations and LOTOS-EUROS model results. J. Geophys. Res. Atmos. 119, 9549–9566. http://dx.doi.org/10.1002/2014JD021911.

Van Damme, M., Erisman, J.W., Clarisse, L., Dammers, E., Whitburn, S., Clerbaux, C., Dolman, A.J., Coheur, P.-F., 2015. Worldwide spatiotemporal atmospheric ammonia (NH_3) columns variability revealed by satellite. Geophys. Res. Lett. 42, 8660–8668, http://dx.doi.org/10.1002/2015GL065496.

Velthof, G.L., van Bruggen, C., Zroenestein, C.M., de Haan, B.J., Hoogeveen, M.W., Huijsmans, J.F.M., 2012. A model for inventory of ammonia emissions from agriculture in the Netherlands. Atmos. Environ. 46, 248-255. http://dx.doi.org/10.1016/j.atmosenv.2011.09.075.

Walker, J., Spence, P., Kimbrough, S., Robarge, W., 2008. Inferential model estimates of bi-directional ammonia dry deposition in vicinity of a swine production facility Atmos. Environ. 42, 14, 3407–3418. http://dx.doi.org/10.1016/j.atmosenv.2007.06.004.

Wang, L., Xu, Y., Schjoerring, J.K., 2011. Seasonal variation in ammonia compensation point and nitrogen pools in beech leaves (Fagus sylvatica). Plant Soil 343, 51-66. http://dx.doi.org/10.1007/s11104-010-0693-7.

Wang, L., Ibrom, A., Korhonen, J.F.J., Frumau, K.F.A., Wu, J., Pihlatie, M., Schjoerring, J.K., 2013. Interactions between leaf nitrogen status and longevity in relation to N cycling in three contrasting European forest canopies. Biogeosciences 10, 999-1011. http://dx.doi.org/10.5194/bg-10-999-2013.

Wentworth, G.R., Murphy, J.G., Benedict, K.B., Bangs, E.J., Collett Jr,J.L., 2016. The role of dew as a nighttime reservoir and morning source for atmospheric ammonia. Atmos. Chem. Phys. 16, 7435-7449. http://dx.doi.org/10.5194/acp-16-7435-2016.

Wichink Kruit, R.J., van Pul, W.A.J., Sauter, F.J., van den Broek, M., Nemitz, E,. Sutton, M.A., Krol, M., Holtslag, A.A.M., 2010. Modeling the surface-atmosphere exchange of ammonia. Atmos. Environ. 44, 945-957. http://dx.doi.org/10.1016/j.atmosenv.2009.11.049.

Wichink Kruit, R.J., Schaap, M., Sauter, F.J., van Zanten, M.C., van Pul, W.A.J., 2012. Modeling the distribution of ammonia across Europe including bi-directional surface-atmosphere exchange. Biogeosciences 9, 5261-5277. http://dx.doi.org/10.5194/bg-9-5261-2012.

Wu, J., van der Linden, L., Lasslop, G., Carvalhais, N., Pilegaard, K., Beier, C., Ibrom, A., 2012. Effects of climate variability and functional changes on the interannual variation of the carbon balance in a temperate deciduous forest. Biogeosciences 9, 13-28. http://dx.doi.org/10.5194/bg-9-13-2012.

Wu, Z., Wang, X., Chen, F., Turnipseed, A.A., Guenther, A.B., Niyogi, D., Charusombat, U., Xia, B., Munger, J.W., Alapaty, K., 2011. Evaluating the calculated dry deposition velocities of reactive nitrogen oxides and ozone from two community models over a temperate deciduous forest. Atmos. Environ. 45, 2663-2674. http://dx.doi.org/10.1016/j.atmosenv.2011.02.063.

Zhang, L., Wright, L.P., Asman, W.A.H., 2010. Bi-directional air-surface exchange of atmospheric ammonia: A review of measurements and a development of a big-leaf model for applications in regional-scale air-quality models. J. Geophys. Res. -Atmos. 115, D20310. http://dx.doi.org/10.1029/2009JD013589.

Table 1: Site location and characteristics during the measurement periods. Mean including standard deviation is given for *PAI*, temperature and rain.

		MMSF	**DK-Sor**
Lat/Lon		39°53’N, 86°25’W	55°29’N, 11°38’E
Forest type		Temperate deciduous, mixed	Temperate deciduous, beech
Canopy height	m	~28	~26
Tree age	years	80 - 90	82
Summer *PAI*	$m^2\ m^{-2}$	4.6	4.6
Soil type		Mesic Typic Dystrochrepts	Alfisols or Mollisols
Leaf N status	%	2.2	2.5
Measurement period			
Dates		5 - 10 September 2013	21 October – 15 November 2010
DOY		248 – 253	294 – 319
Mean *PAI*	$m^2\ m^{-2}$	4.5 ± 0.0	2.2 ± 0.9
Mean Temp.	ºC	24.5 ± 3.3	6.7 ± 2.6
Total Rain	mm	12.8	124.0

Table 2: List of input parameters for the SURFATM-NH_3 model for the MMSF and DK-Sor model setups. Pedotransfer functions applicable to Danish soil types are used (Madsen and Holst 1988) and some soil parameters for the DK-Sor site were measured in the NitroEurope project (2006-2011) and provided from there.

	Soil parameters	**Unit**	**Range**	**MMSF/DK-Sor**	**Source**
	Soil depth	m		0.86 / 0.80	Thompson et al. (2011) / NitroEurope IP
	Soil density	kg m^{-3}		1220 / 1038	Measured / NitroEurope IP
	Soil humidity at field capacity	kg (H_2O) kg^{-1} (soil)	[0.15 – 0.4]	0.36 / 0.36	Estimated / calculated using pedotransfer function
	Soil humidity at wilting point	kg (H_2O) kg^{-1} (soil)	[0.05 – 0.25]	0.22 / 0.24	Estimated / calculated using pedotransfer function
	Thermal soil conductance (wet)	W m^{-1} K^{-1}	[1.6 – 2.2]	1.60 / 1.00	Monteith and Unsworth (1990)
	Thermal soil conductance (dry)	W m^{-1} K^{-1}	[0.2 – 0.3]	0.28	Monteith and Unsworth (1990)
	Soil porosity	-	[0.25 – 0.5]	0.55	Thompson et al. (2011) / Estimated
	Soil tortuosity parameter	-	[2 - 4]	2.00	Estimated
	Soil Roughness	m	[0.001 – 0.5]	0.02	Estimated
	Chemical constants				
K_H	Henry Constant for NH_3	-		$10^{-3.14}$	Loubet (2000)
K_d	Dissociation constant for acid-base dissociation NH_4^+/NH_3	mol l^{-1}		$10^{-9.25}$	Bates and Pinching (1950)
	Vegetation parameters				
	Leaf width	m	[0.03 – 0.5]	0.15 / 0.10	Measured
	Canopy height	m		28 / 26	Measured
	Max stomatal conductance	m s^{-1}		400	Collatz et al. (1991)
	Efficiency coefficient for plant area index			0.25	Estimated
	Radiation attenuation coefficient	-	[0.5 – 0.8]	0.80 / 0.85	Estimated / calculated using radiation data
	Wind attenuation coefficient	-	[1.5 - 5]	2.20	Estimated
	Ammonia emission potentials				
$\Gamma_{g,min}$	Min ground layer emission potential	-		300	Estimated
$\Gamma_{g,max}$	Max ground layer emission potential	-		18000	Estimated
Γ_s	Leaves (stomata)	-	[0 - 600]	400 / 200	Estimated / Wang et al. (2011)

Table 3: Model error statistics including the number of valid observations, *n*, Pearson correlation coefficient, R^2, root mean squared error, *RMSE*, and the Concordance coefficient, *CCC* (in W m^{-2} for energy fluxes and µg NH_3-N m^{-2} s^{-1} for ammonia fluxes). See text (section 3.1.1) and Figure 3 for energy balance closure.

MMSF	*n*	R^2	*RMSE*	*CCC*
H	240	0.78	59.17	0.69
LE	240	0.87	71.83	0.78
G	240	0.40	21.46	0.22
F_{NH3}	209	0.51	14.03	0.43
DK-Sor	*n*	R^2	*RMSE*	*CCC*
H	1198	0.17	71.94	0.14
LE	1199	0.07	37.32	0.04
G	1200	0.65	10.97	0.32
F_{NH3}	1020	0.62	94.29	0.60

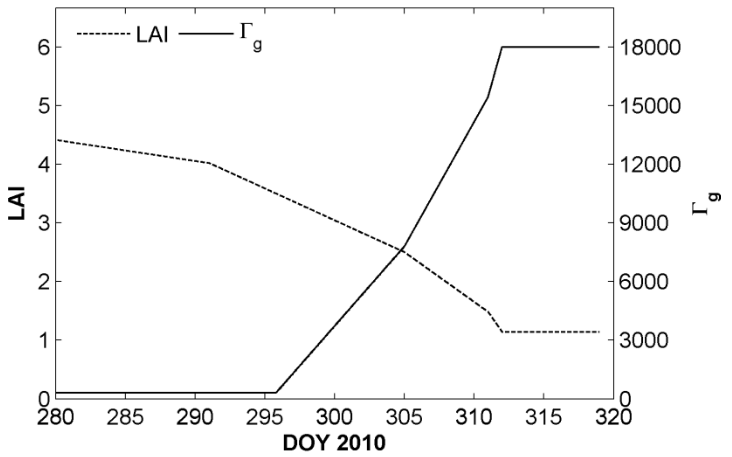

Figure 1: Parameterization of the ground layer emission potential $\Gamma_g = [NH_4^+]/[H^+]$ with the decrease in $\Delta LPAI$ exemplified using *PAI* data from the DK-Sor site.

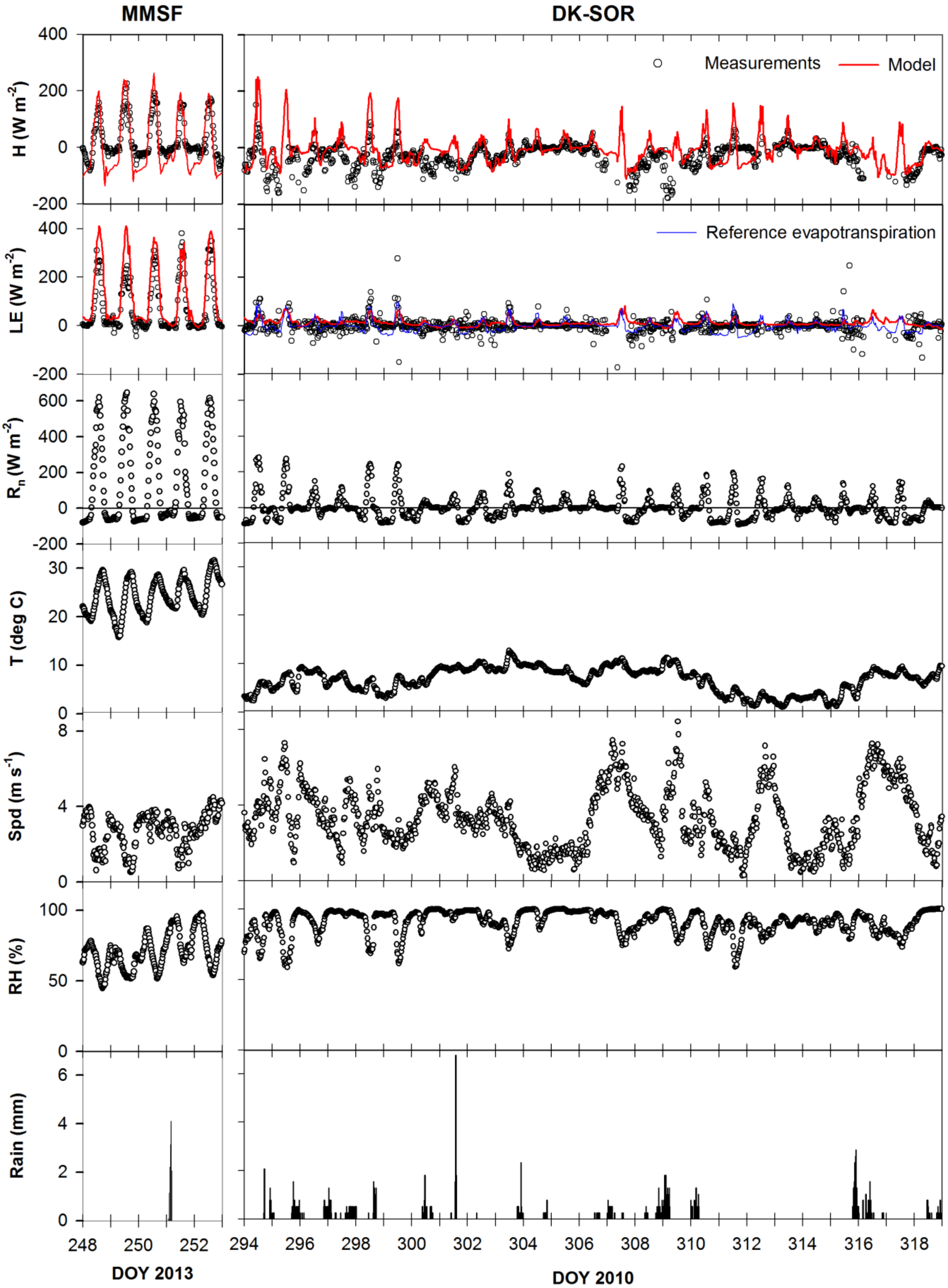

Figure 2: Comparison of the measured (dots) and the simulated (red lines) energy fluxes (W m^{-2}) of sensible heat (*H*) and latent heat (*LE*) for the MMSF and DK-Sor sites. For the DK-Sor site the FAO Penman-Monteith reference evapotranspiration is also shown with (blue line). Measurements of net radiation, *Rn* (W m^{-2}), air temperature, *T* (degree celcius), wind speed, *Spd* (m s^{-1}), relative humidity, *RH* (%), and *rain* (mm) are shown in the lowest graphs.

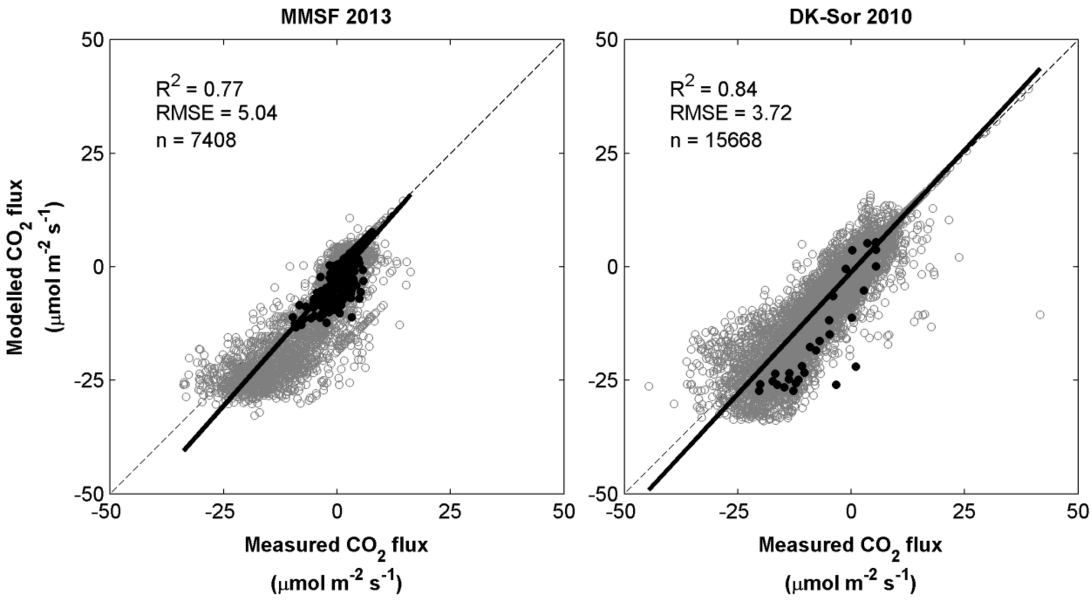

Figure 3: Scatterplot of the modelled vs. the measured CO_2 flux (µmol m^{-2} s^{-1}) for the DK-Sor site for the full year of 2010 (left) and for the MMSF site for the full year of 2013 (right). Black filled symbols show the data points during the measurement periods. *R^2* is the coefficient of determination, *RMSE* is the root mean square error, and *n* is the number of valid sampling points.

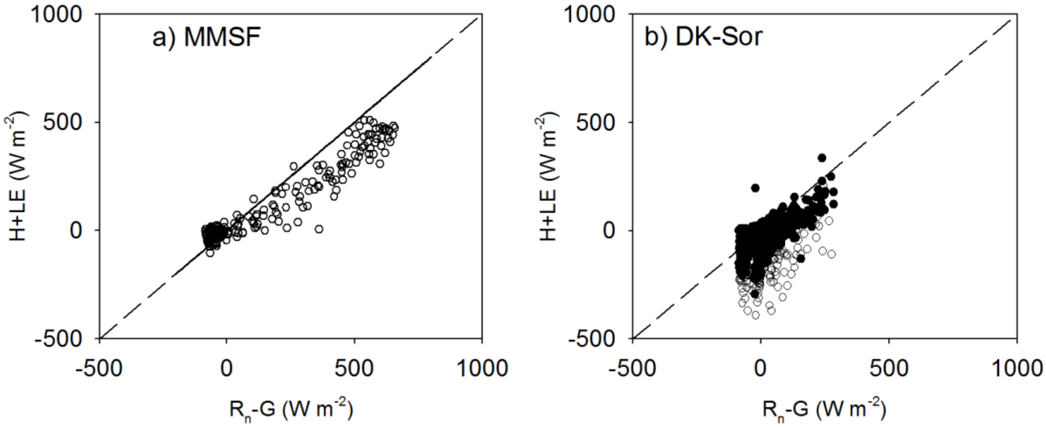

Figure 4: Scatter plots comparing the measured available energy (*Rn* – *G*) to the measured turbulent energy fluxes (*H* + *LE*) for a) the MMSF site and b) the DK-Sor site during the measurement periods. For (b) the filled circles indicate measurements during periods where the wind speed was 0-5 m s^{-1} and the open circles represent data measured at wind speeds higher than 5 m s^{-1}.

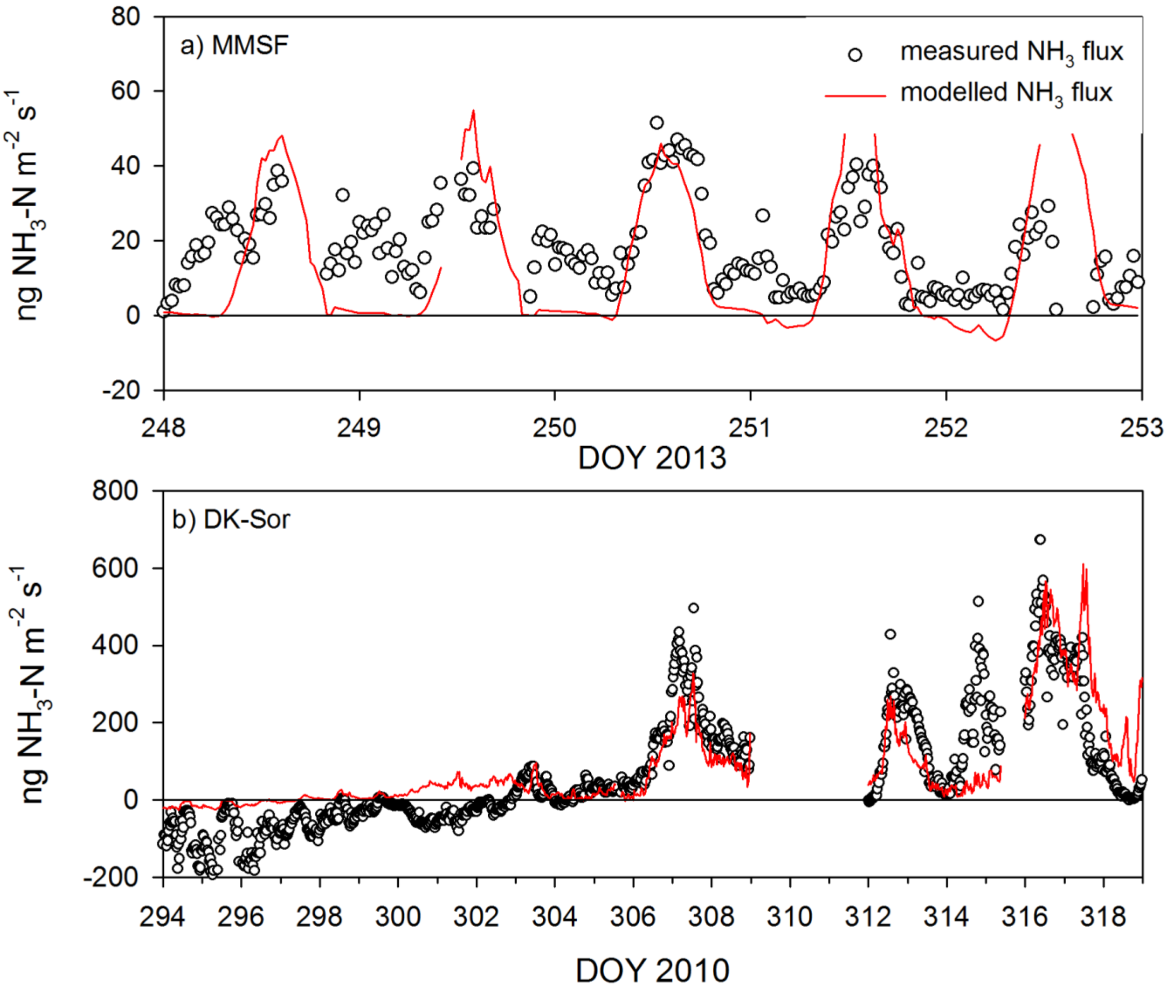

Figure 5: Comparison of the measured (dots) and the simulated (lines) NH_3 fluxes (ng NH_3 m^{-2} s^{-1}) for a) the MMSF site and b) the DK-Sor site during the measurement periods.

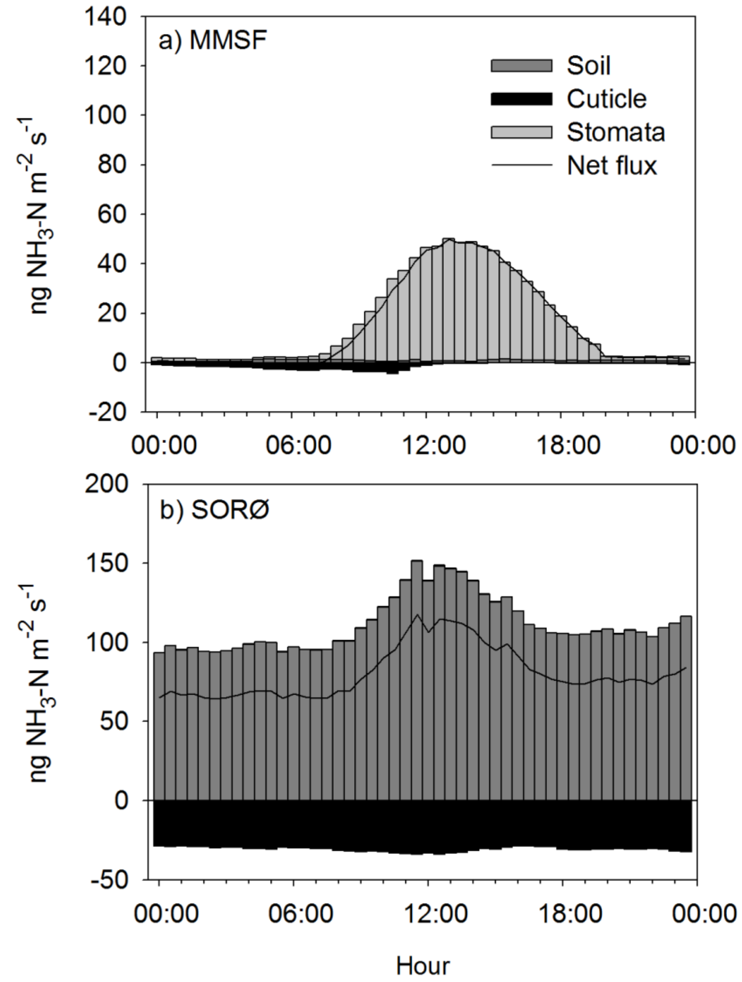

Figure 6: Simulated mean forest component fluxes (ng NH_3-N m^{-2} s^{-1}) from the ground layer (light grey), cuticles (dark grey), and stomata (white) for a) MMSF site, which represents a green canopy and b) DK-Sor site, which represents the leaf fall period. The solid line shows the mean NH_3 net flux (ng NH_3-N m^{-2} s^{-1}).

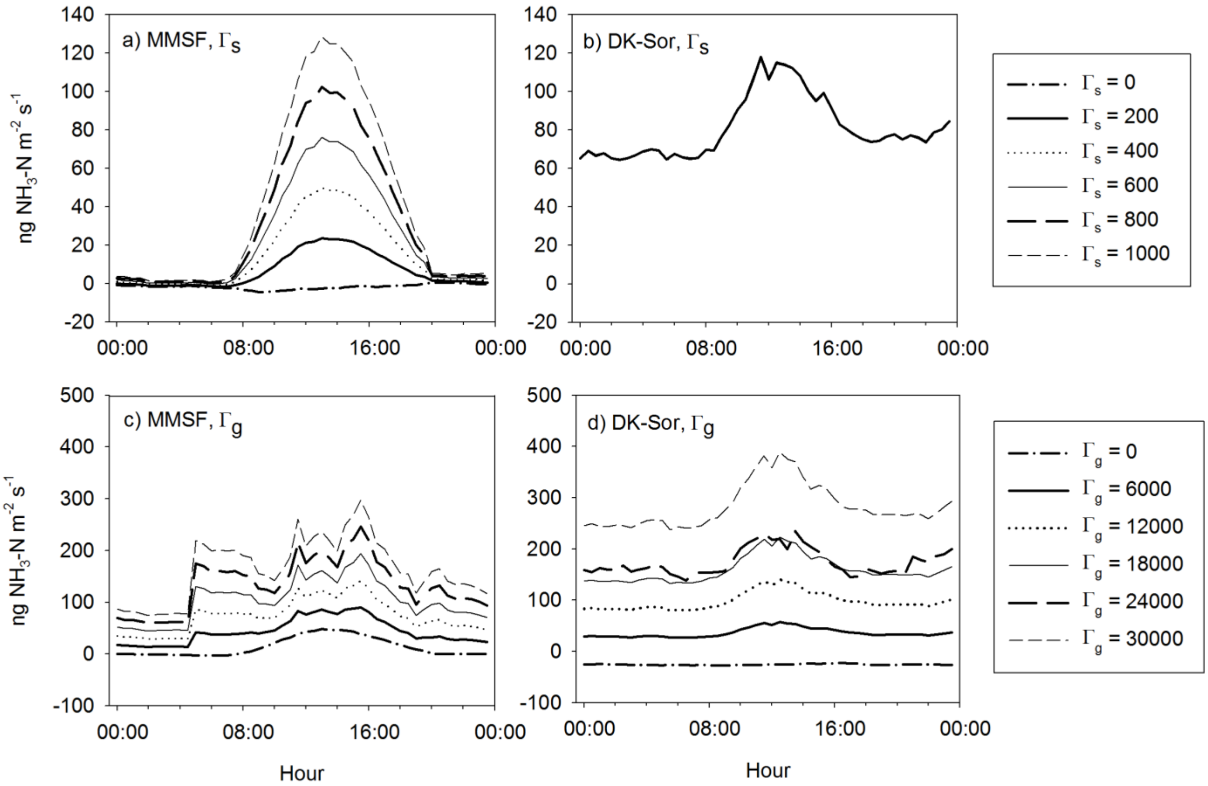

Figure 7: The simulated mean NH_3 flux (ng NH_3-N m^{-2} s^{-1}) for a green forest canopy (MMSF) and for a leaf fall forest canopy (DK-Sor) with different stomata emission potentials (Γ_s) (a and b) and different ground layer emission potentials (Γ_g) (c and d). In panel b) all results fall on one single line, indicating that the stomatal NH_3 pathway is negligible.